

# FACE GENERATION AND EDITING WITH STYLEGAN: A SURVEY

<b>1</b>	<b>Introduction</b>	<b>1</b>
1.1	Survey Overview . . . . .	1
1.2	Synopsis of StyleGAN Applications . . . . .	1
<b>2</b>	<b>StyleGAN Architectures for Generation of Faces</b>	<b>3</b>
2.1	Generative Adversarial Networks . . . . .	3
2.2	Progressive growing GANs (PGGAN) . . . . .	3
2.3	StyleGAN . . . . .	3
2.4	StyleGAN2 . . . . .	4
2.5	StyleGAN3 . . . . .	4
2.6	Training datasets . . . . .	5
<b>3</b>	<b>Measuring Similarity of Faces</b>	<b>5</b>
3.1	The $L_2$ Loss . . . . .	5
3.2	The LPIPS Loss . . . . .	5
3.3	Identity Preservation Loss . . . . .	6
3.4	Fréchet Inception Distance FID . . . . .	6
<b>4</b>	<b>Latent Spaces of StyleGAN</b>	<b>6</b>
4.1	$\mathcal{Z}$ and $\mathcal{Z}+$ spaces . . . . .	7
4.2	$\mathcal{W}$ space . . . . .	7
4.3	$\mathcal{W}+$ space . . . . .	7
4.4	$\mathcal{S}$ space . . . . .	7
<b>5</b>	<b>GAN Inversion to Latent Spaces of StyleGAN</b>	<b>8</b>
5.1	Major groups of inversion methods . . . . .	8
5.2	Evaluating GAN Inversions . . . . .	9
5.3	Inversion Encoders . . . . .	10
5.4	Fine-tuning of the StyleGAN generator for better inversion . . . . .	11
<b>6</b>	<b>Editing Face Images with StyleGAN</b>	<b>12</b>
6.1	Global semantic directions . . . . .	12
6.2	Single image semantic directions . . . . .	14
<b>7</b>	<b>Cross Domain Face Stylization with StyleGAN</b>	<b>14</b>
7.1	CLIP-Guided Domain Adaptation of StyleGAN . . . . .	14
7.2	Layer Swapping for Controllable Domain Adaptation . . . . .	15
7.3	Blending for Stylized Face Generation . . . . .	15
7.4	Caricature Generation via StyleGAN Feature Map Modulation . . . . .	15
<b>8</b>	<b>Face Restoration with StyleGAN</b>	<b>16</b>
8.1	GAN Prior Embedded Network for Blind Face Restoration in the Wild . . . . .	16
8.2	GFP-GAN: Towards Real-World Blind Face Restoration with Generative Facial Prior . . . . .	16
8.3	MyStyle: A Personalized Generative Prior . . . . .	17
<b>9</b>	<b>Deepfakes</b>	<b>17</b>
9.1	Facial Reenactment . . . . .	17
9.2	Face Replacement and Face Transfer . . . . .	18
<b>10</b>	<b>Conclusion</b>	<b>18</b>
	<b>References</b>	<b>19</b>

# Face Generation and Editing with StyleGAN: A Survey

Andrew Melnik, Maksim Miasayedzenkau, Dzianis Makarovets, Dzianis Pirshtuk, Eren Akbulut, Dennis Holzmann, Tarek Renusch, Gustav Reichert, and Helge Ritter

**Abstract**—Our goal with this survey is to provide an overview of the state of the art deep learning technologies for face generation and editing. We will cover popular latest architectures and discuss key ideas that make them work, such as inversion, latent representation, loss functions, training procedures, editing methods, and cross domain style transfer. We particularly focus on GAN-based architectures that have culminated in the StyleGAN approaches, which allow generation of high-quality face images and offer rich interfaces for controllable semantics editing and preserving photo quality. We aim to provide an entry point into the field for readers that have basic knowledge about the field of deep learning and are looking for an accessible introduction and overview.

**Index Terms**—StyleGAN, GAN, Face Generation, Computer Vision, Similarity Measures, Latent Models, Deep Learning, Deepfakes.

## 1 INTRODUCTION

HUMANS have always been fascinated with faces. It is how we recognize people, it is the main feature we watch out for when interacting with other people. This is reflected in the fact that we have a specialized region in our brain solely dedicated to the detection of face patterns and their subtle changes [16] [17].

There are almost 8 billion people alive today and yet we can discern all of them by their face. Attempting to delineate the great diversity of faces, [18] proposes 26 facial features as relevant for the description of faces (including many shape and size features, along with features for color and texture). Giving each of these features as few as only three value levels already leads to  $3^{26} > 2.5 \cdot 10^{12}$  different faces, which is about 300 time bigger number than the number of people alive today. Thus, there is still a vast space for unique identification of individuals using facial features.

Our goal with this survey is to provide an overview of the state of the art deep learning technologies for face generation and editing. We particularly focus on GAN-based architectures that have culminated in the StyleGAN approaches, which allow generation of high-quality face images and offer rich interfaces for controllable semantics editing and preserving photo quality. The StyleGAN architecture merits the attention of a broader readership because it provides an ecosystem for a variety of applications [19] and is used as the basis for a large number of research works. For a condensed visual synopsis, see Figure 1 and Chapter 1.2.

### 1.1 Survey Overview

The plan of the paper is as follows: Chapter 1.2 attempts to give an impression of the richness of applications of StyleGAN-based image processing methods. Chapter 2 will

explain Generative Adversarial Networks (GANs), delving specifically into the StyleGAN architectures for the generation of face images. Training such architectures needs suitable metrics that capture image similarity at different levels, which will be the topic of Chapter 3. Chapter 4 will discuss the different latent representations that form the basis of controllable the image editing. Chapter 5 focuses on finding for a given image its latent representation. This prepares the ground for the methods reviewed in Chapter 6 to edit face images, and in Chapter 7 for cross domain face stylization. Finally, in Chapter 8 we look at some major approaches connected with face restoration and producing deepfakes in Chapter 9. The last Chapter 10 concludes with a short summary and outlook.

## 1.2 Synopsis of StyleGAN Applications

### 1.2.1 Synthetic Face Generation

The StyleGAN [5] [3] architecture can generate faces which do not exist (see Figure 1A). There are similar applications of StyleGAN, like creation of unique pieces of art resulted in an non-fungible tokens (NFTs) collection [2] [20] (see Figure 1B). The generative expressiveness of the StyleGAN architecture relies on the dataset used for training. Chapter 2 covers the topic of StyleGAN architectures in more detail.

### 1.2.2 Editing Facial Features

It is possible to create non-existing facial images that share features of both source images (see Figure 1C). Such editing technique, called *style mixing*, is possible by using latent representations of the two images at different layers of the StyleGAN generator (see Figure 3B).

While preserving a high image quality [21], the StyleGAN architecture [3] [22] allows to alter many features like, age, hair, smile and etc. (see Figure 1D and more details in Chapter 6).

The StyleGAN architecture can be used as a component for text-driven editing of images. StyleCLIP [23] [6] offers

- E-mail: andrew.melnik.papers@gmail.com
- A. Melnik, E. Akbulut, D. Holzmann, T. Renusch, G. Reichert, H. Ritter - Bielefeld University, Germany.
- M. Miasayedzenkau, D. Makarovets, D. Pirshtuk - Banuba

Manuscript received November 22, 2022.

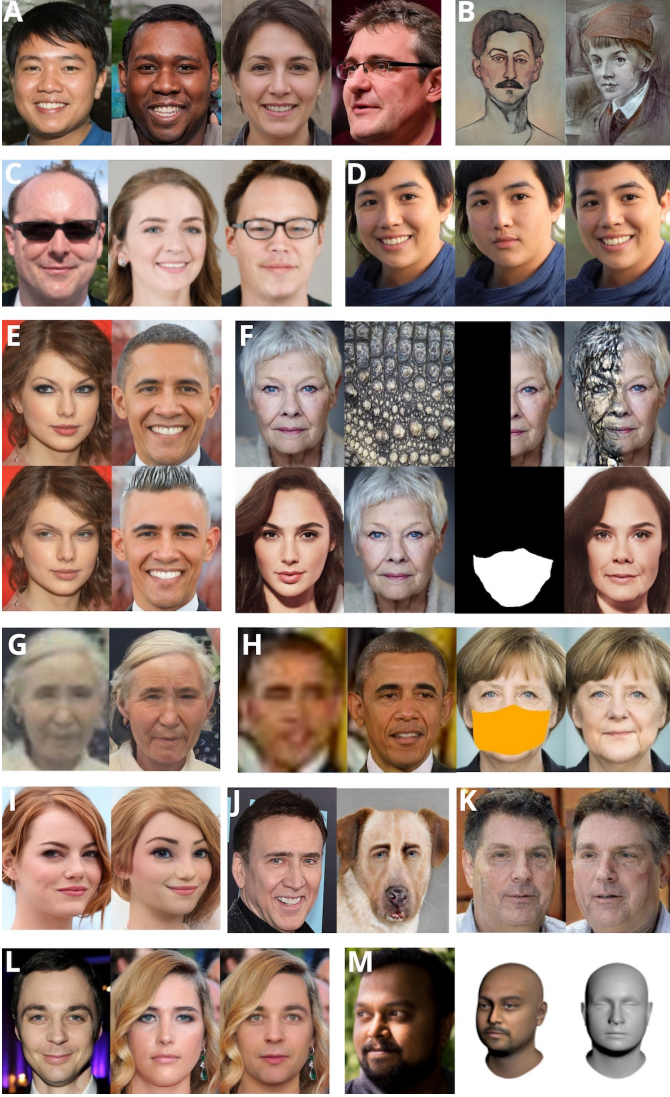


Figure 1: **Synopsis of StyleGAN Applications.** **A.** Faces generated using StyleGAN from website [1]. **B.** NFT collection [2] generated using StyleGAN2 [3] trained on MetFaces dataset [4]. **C.** Style mixing of human faces with StyleGAN. From left to right: the first and the second are the source images, the third is the mixed style image [5]. **D.** Face editing with StyleGAN2. From left to right: the source image, smile removed, gender changed [3]. **E.** Image editing using text prompts with StyleCLIP. Upper row: original images, lower row: edited images using text prompts – Emma Stone (left), Mohawk Style (right) [6]. **F.** Seamless image-crossover using StyleGAN. First column: sources images, last column: resulting merge images [7]. **G.** Blind face restoration using StyleGAN component [8]. Left: degraded image, right: enhanced image. **H.** Identity preserving face restoration and in-painting using StyleGAN component [9] [10]. **I** and **J.** Transferring faces into other domains while preserving the identity using StyleGAN component. Left: real image, right: cartoon like output [11] [12]. **K.** Control interpretable semantic parameters, such as face pose using StyleGAN component. Left: source image, right: pose change [13]. **L.** Deepfake generation [14]. **M.** Automated 3D avatar generation using StyleGAN component. From left to right: source image, avatar, face model [15].

a manipulation of facial features using text prompts alone (see Figure 1E and Chapter 6.2.1).

*Image2StyleGAN++* framework [7] provides application examples of image editing using scribbles, inpainting, crossover (see Figure 1F).

### 1.2.3 Facial Image Recovery

StyleGAN has been demonstrated to be able to restore face images with regard to degradations such as low resolution, noise, colourisation of old photos, and even missing parts (see Chapter 8). For example, GFP-GAN [8] uses a pre-trained StyleGAN2 [3] as a component of the face restoration architecture (see Figure 1G). However using such general facial priors for restoration of images can end up in identity loss of faces. MyStyle [9] tackles the problem of target identity, while recovering lost information (see Chapter 8.3 and Figure 1H)

### 1.2.4 Cartoonization of Faces

Creating copies of face images in another domain while preserving the person identity is a big challenge. The goal of cartoonization approaches [24] [25] [26] is to satisfy both identity preservation and perceptual features of a certain cartoon style (see Figure 1I and 1J for example applications and Chapter 7 for technical details).

### 1.2.5 3D Facial Avatar Generation

StyleGAN has been shown to be useful for transferring a 2D human face images to a 3D avatar, while preserving identity [15](see Figure 1M). Such 3D avatars can be useful e.g., in gaming, real time video filters, etc. In addition, this transfer can be made within domain changing, for example from real world to cartoon domain [25].

### 1.2.6 Deepfake generation

Deepfake generation can be summed up as a face-swapping operation that is not being recognizable by human viewers (see Figure 1L). Deepfakes are used by artists, social media platforms, in film, game, fashion, and entertainment industry [27] [28] [29] [30]. Many deepfake creation approaches for static images are applicable to videos as well. See Chapter 9 for details on leveraging of StyleGAN functionality for deepfake applications: face reenactment [31] [32], swapping [14], and transfer [33].

### 1.2.7 Hands-on Applications and Mobile Networks

Face generation and editing technologies are popular for social networks, messengers, mobile and photo apps. In many cases, privacy issues motivate the localisation of processing from cloud servers to mobile devices. Mobile architecture networks [34] are constrained to being fast while consuming only little memory on the order of a few megabytes (MB) instead of several gigabytes.

Although the functionality and applications of StyleGAN are very diverse, running architectures that include the StyleGAN model can be computationally demanding. Thus, in many cases the StyleGAN architecture can be used to generate a dataset of paired examples. This dataset can be used for supervised learning of lightweight architectures, which require small computational resources and



have a discrete specialized functionality. That means, it is necessary to train a separate such mobile encoder-decoder network (e.g., 1-10 MB) for each editing feature like adding glasses, smile, makeup etc. Such mobile networks are usually trained using supervised learning with training pairs generated from full size architectures [35] [36].

## 2 STYLEGAN ARCHITECTURES FOR GENERATION OF FACES

To generate images of faces, GANs have proven to be a highly suitable architecture. We first briefly sketch the underlying idea of the approach and then delve into its recent refinements, leading to the succession of StyleGAN architectures [5] [3] [22] that revolutionized high quality face image generation and that have become the current state of the art in the field.

### 2.1 Generative Adversarial Networks

Generative adversarial networks (GAN) offer a way to learn a mapping that transforms a known, usually simple (e.g. Gaussian) distribution into a more complex target distribution that represents a given domain of patterns, for example, images of human faces. This mapping or generative model can be learnt using a sufficiently large training set of samples from the desired target distribution. Once the model has been learnt, new samples can be generated by simply feeding the model with random inputs from the simple distribution that was used during training.

A GAN model [37] is comprised of two networks, the **generator** and the **discriminator**. The generator has to learn to transform samples from a known distribution (e.g. a multidimensional Gaussian with unit variance in all directions) into samples that matches a given target distribution as closely as possible. This is achieved by linking the training of the generator in an “adversarial” manner with the simultaneous training of the discriminator: the latter is fed with a sequence of images that are either sampled from the given training set (“true images”) or generated by the generator (“fake images”). The discriminator is given the goal to distinguish the true images from the fakes, while the generator is given the goal to make its fakes for the discriminator as indistinguishable from the true images as possible. Therefore, the generator and discriminator are competing against each other: while the generator tries to fool the discriminator by generating artificial images which look like the images from the training dataset, the discriminator seeks to differentiate as well as possible between images from the dataset and artificial images generated by the generator. Computationally, this competition is cast into a particular loss function, the GAN-loss that is the subject of the next subsection.

#### 2.1.1 Adversarial Loss

Adversarial loss forms the basis for building generative adversarial models [37]. We denote the generator network that learns to generate samples from some data distribution by  $G$ , and the discriminator network that learns to determine whether a sample is from real data distribution or not by  $D$ . Let  $G(z)$  be an image which generated from

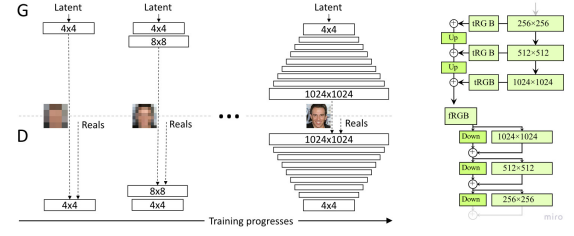


Figure 2: (a) StyleGAN grows progressively while training, (b) StyleGAN2 does not but uses output skips and residual connections [41]

sample  $z$  in a known distribution  $p_z$  and  $D(x)$  be the probability of  $x$  being drawn from the data distribution  $p_{data}$  rather than generator one. Then, the training objective of  $D$  is to discriminate real images from generated one. This requires to maximize  $D(x)$ , when  $x$  is sampled from  $p_{data}$ . However, when  $x = G(z)$  is produced by the generator, the generator wants to see  $D(G(z))$  maximized. Switching to  $\log(1 - D(G(z)))$  reverses the optimization direction for both  $D$  and  $G$ , allowing to express the adversarial training of  $D$  and  $G$  as the optimization of a two-player minimax game with value function  $V(G, D)$  give as [37]:

$$\min_G \max_D V(G, D) = \mathbb{E}_{x \sim p_{data}(x)} [\log D(x)] + \mathbb{E}_{z \sim p_z(z)} [\log(1 - D(G(z)))].$$

This is the basic loss function for training GANs, but using the minimax loss can cause a training instability. Other loss functions such as Wasserstein GAN loss [38], Hinge loss [39], non-saturating loss [37] have been found to improve the stability of GANs training in many situations.

### 2.2 Progressive growing GANs (PGGAN)

While vanilla GANs are able to generate images of reasonable quality, they suffer from limited controllability and unstable training [40]. To overcome these problems, Karras et al. [41] introduced a training strategy in which the neural network progressively grows more layers during training (see Figure 2a). With layers at increasing depth, image resolution increases as well. Starting with low-resolution images of  $4 \times 4$  up to a resolution of  $1024 \times 1024$ , firstly coarse structures and later fine details are learned. This makes training more stable, because it splits the task into simpler sub-tasks. Additionally, the training time benefits from this approach, because most of the iterations are done at lower resolutions and thus in a network with a smaller number of layers.

### 2.3 StyleGAN

StyleGAN [5] adapts the progressive training strategy from the PGGAN [41] and the generator architecture is re-designed motivated by the style transfer ideas [42]. As a result, it offers a high degree of flexibility to mix image styles at different levels of its generator architecture.

StyleGAN no longer passes the random sample  $z$  (often referred to as *latent code* for being “decoded” by the generator) directly into the generator’s input layer. Instead, StyleGAN starts generating images from a learned constant



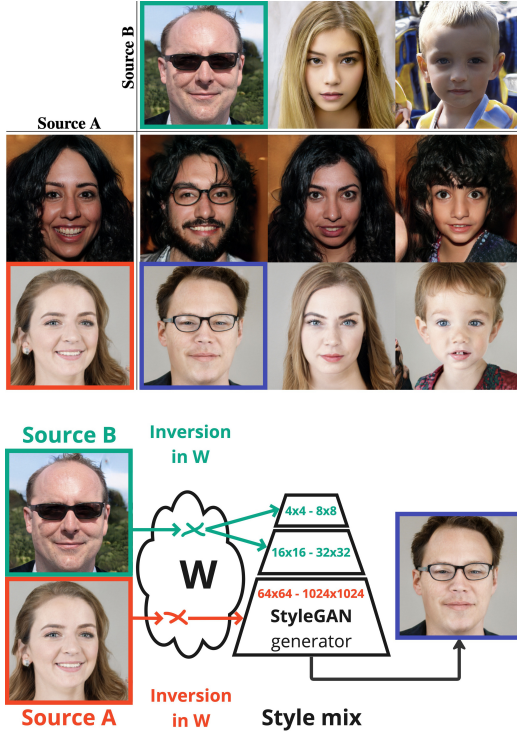


Figure 3: Style mixing in StyleGAN [5] : a) shows examples of style mixing, b) illustrates how different styles can be used in different levels of the generator

( $4 \times 4 \times 512$ ), and the latent code  $z \in \mathcal{Z}$  is fed into the network along a different route. It first is mapped through a deep network of fully connected layers into an intermediate latent space  $w \in \mathcal{W}$ . The benefit of this  $\mathcal{Z}$  to  $\mathcal{W}$  transformation is that the intermediate space  $\mathcal{W}$  does not need to follow the distribution of the training data ( $\mathcal{Z}$  however does). Thus,  $\mathcal{W}$  can be disentangled which is a desirable property because it means that later, features in the generated images can be controlled independently of each other. Subsequently, and for each generator layer separately, it is converted into a vector of style parameters that are used to shift and scale the activity pattern in the feature maps of the respective convolutional layer. This affine transformation of feature maps is called an adaptive instance normalization (AdaIN) [42].

This layer-wise feeding of style parameters allows style-mixing by feeding code parameters  $w_A$  and  $w_B$  of two sources A and B respectively into different layer subsets of the StyleGAN generator (see Figure 3). If a code is injected into early layers it affects rough features while injection into later layers correspond to finer details. Finally, to provide stochastic detail that would have to be learned otherwise, pixel-wise noise is injected after each convolution. This allows the network locally stochastic placing of fine structure, such as pores, hairs, or freckles.

## 2.4 StyleGAN2

StyleGAN was a major breakthrough towards the generation of high-resolution face images that looked very natural. Yet, the generated images tended to contain minor, but systematic artifacts, such as blobs or droplets. A careful analysis of this phenomenon enabled the development of an updated version, StyleGAN2 [3].

Its key change was a simplification and reorganisation of the layer normalization, which in the original StyleGAN was recognized as destroying information in the relative activation strengths of the different feature maps within a layer. This was avoided by replacing the former AdaIN operations by a direct rescaling of the convolutional weights, again based on the the style parameter output associated with  $w$ , followed by a normalization by the standard deviation over the scaled weights. Additionally, the noise and bias now became added outside the style block and removed from the initial learned constant input.

Another problem was that in the images created by StyleGAN some details like eye or teeth orientation seemed to be either stuck in place or jumping between positions instead of moving smoothly. This was attributed to the generator needing to produce output images at each resolution, which forces it to generate maximal frequency details. To overcome this problem, StyleGAN2 no longer trains models using progressive growing, but sums the output from different resolutions together and utilizes skip connections (see Figure 2b). The size of the model itself was also increased through the number of feature maps in the layers responsible for the highest resolutions.

Furthermore, a new regularization loss was introduced to control the perceptual path length (PPL), which quantifies the smoothness of the mapping from a latent space to the output image by measuring average LPIPS (see chapter 3.2) between generated images under small perturbations in latent space. It is assumed that lower PPL correlates with higher image quality and better editability.

## 2.5 StyleGAN3

While StyleGAN2 abolished the above artifacts and further increased image quality by a number of measures, a remaining problem was that, when interpolating between two images fine details appeared to be stuck to specific image coordinates instead of properly co-moving with the object surfaces to which they were attached. For example, hairs stick to certain pixels during such a transition instead of to the skin. It turned out that the network had a strong propensity to fix a feature to image coordinates whenever any information about such coordinates was available to the network. Major sources of such information turned out to be image borders and aliasing patterns from discretization on a pixel grid. The first problem could be overcome by sufficient zero padding around the image in the generator [43]. The discretization problem was overcome by reformulating all operations for a continuous image, but with spatial frequency content band-limited to allow a lossless equivalence to a pixel grid of values, which then could be used as an equivalent representation. Correct maintenance of this equivalence required a careful enclosing of the application of the non-linearity between upsampling and downsampling operations designed to filter away any spectral out-of-band contents otherwise introduced by the non-linearity. Further changes introduced in the StyleGAN3 architecture [22] included an optimized reduction of the number of layers and simplifications, including retracting some regularizations that were introduced in StyleGAN2 but incompatible with a strict enforcement of translation invariance.

These changes are listed below and lead to images that are equivariant to translation and rotation, which is especially useful for video and animation [22].

**Fourier features:** the learned  $4 \times 4 \times 512$  constant used in StyleGAN2 is replaced by randomly generated and information-wise equivalent Fourier features with dimensionality  $36 \times 36 \times 1024$  as the first layer.

**Transformed Fourier features:** A learned affine layer is introduced that outputs global translation and rotation parameters for the new input Fourier features.

**Simplified generator:** StyleGAN3 no longer uses added in noise, reduces the number of layers from 18 to 14 and disables mixing regularization and PPL regularization.

**Boundaries:** To prevent leakage of absolute image coordinates into the internal representations, a fixed-size margin around the target canvas, that is cropped after each layer, is introduced to replace the previously used padding.

**Up & down-sampling:** up and down-sampling operations were modified to prevent the leak of pixel coordinates through aliasing artifacts.

**Filtered non-linearities:** Nonlinearities such as ReLU introduce high frequency information that leads to aliasing which is fixed by upsampling before and downsampling after applying the nonlinearity and vice versa.

**Non-critical sampling:** StyleGAN3 [22] also uses lower cutoff frequencies for filters during up-sampling and down-sampling operations to eliminate aliasing.

**Flexible layers:** By setting different filter parameters for each layer individually, translation equivariance is improved.

**Rotational equivariance** is achieved by replacing  $3 \times 3$  convolutions with  $1 \times 1$  convolutions, and replacing cartesian downsampling filters with radially symmetric ones for all layers except the last two.

## 2.6 Training datasets

Large data sets are an extremely important resource for training deep networks, with GANs being no exception. The majority of the approaches discussed in this survey used the following two datasets for training: FFHQ [44] [5] and CelebA-HQ [45].

**Flickr-Faces-HQ (FFHQ)** is a high-quality image dataset of human faces, originally created as a benchmark for generative adversarial networks (GAN). The dataset consists of 70,000 high-quality PNG images at  $1024 \times 1024$  resolution and contains considerable variation in terms of age, ethnicity and image background. It also has good coverage of accessories such as eyeglasses, sunglasses, hats, etc. The images were crawled from Flickr, thus inheriting all the biases of that website, and were automatically aligned and cropped using dlib [46].

**CelebFaces Attributes Dataset (CelebA-HQ)** is a large-scale face attributes dataset with more than 200K celebrity images, each with 40 attribute annotations. The images in this dataset cover large pose and background variations. CelebA is diverse, large, and has rich annotation, including 10.177 identities, 202.599 face images, 40 binary attribute annotations and 5 landmark locations (eyes, nose, mouth) per image.

## 3 MEASURING SIMILARITY OF FACES

Providing tools for face generation and editing is intimately linked with the question how to align computational similarity measures for face images with human perception and judgement. We already saw that faces are connected with numerous dimensions along which their similarity and semantic contents can vary. Moreover, many of these dimensions are at least partly subjective. This chapter discusses several loss functions that are relevant for evaluating the quality of generated images.

### 3.1 The $L_2$ Loss

The  $L_2$  loss measures pixel-wise similarity between two images  $x$  and  $\hat{x}$ . It is defined as  $L_2(x, \hat{x}) = \sum_i (x_i - \hat{x}_i)^2$ .

While this is a fairly simple way to compute the similarity between two images, it suffers from the drawback that such pixel-wise comparison is insensitive to the local context of image points. This can make the  $L_2$  distance very different from human image similarity judgements [47]. For example, for an image with a white horizontal line on a black background. If we shift the horizontal line just by one pixel down, the  $L_2$  distance will be large, but the two images might be indistinguishable to a human. Constructing a human-like perception metric is challenging because human judgments of similarity depend upon many factors, including high-order image structure, context and visual experience.

### 3.2 The LPIPS Loss

One way to go beyond the shortcomings of simple image pixel comparisons as in the  $L_2$  measure is to transform the images into a space, whose point-wise distance reflects human similarity judgements better and to apply a  $L_2$  measure there. This is the underlying idea of the Learned Perceptual Image Patch Similarity (LPIPS) [48] measure. As image transformation it uses CNNs that were trained to solve visual recognition tasks, such as VGG [49] or AlexNet [50]. The activations of these networks are known to represent a hierarchy of increasingly abstract image features, motivating to compute the similarity measure for an image pair  $x, \hat{x}$  as a weighted sum of  $L_2$  distances between the corresponding feature map activations  $y^l, \hat{y}^l$  with shape  $(H_l, W_l, C_l)$  in the hidden layers  $l$ . The weighting coefficient  $w_l$  scales the activations channelwise and provides parameters to further adjust the metric (in addition to the prior DNN training) to make it match human similarity judgements on a data base of image pairs as faithfully as possible. The LPIPS metric thus takes the form:

$$d(x, \hat{x}) = \sum_l \frac{1}{H_l W_l} \sum_{h,w} \|w_l \odot (y_{hw}^l - \hat{y}_{hw}^l)\|_2^2.$$

The intuition is, that CNN features in a DNN model supply a more abstract representation of a given picture. As a result, distances in this representation space are better reflecting what is relevant for making images appear different and are less sensitive to low-level perturbations when these are irrelevant to image content.

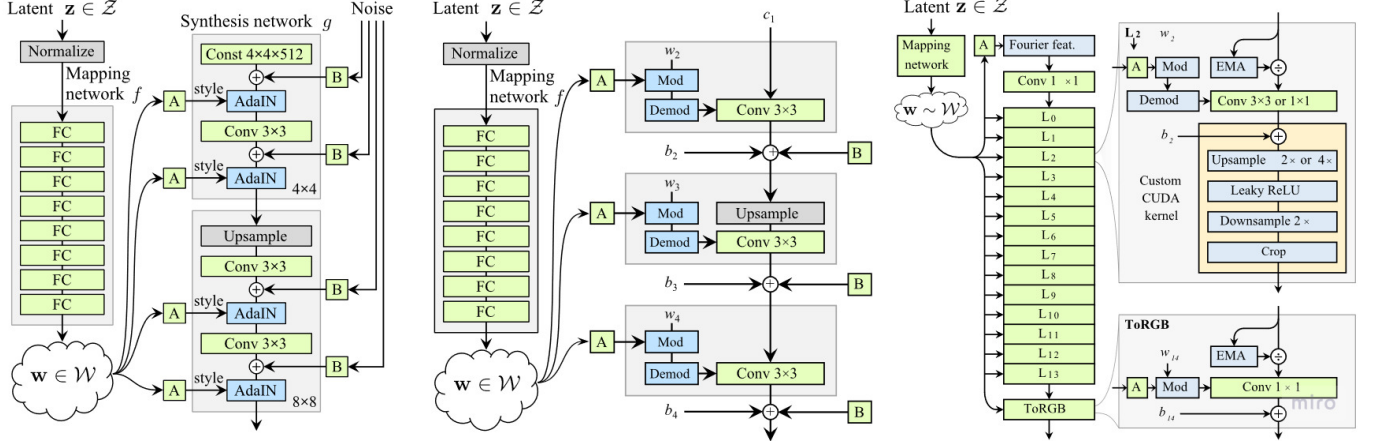


Figure 4: Architectures of StyleGAN generators: (a) StyleGAN, (b) StyleGAN2, (c) StyleGAN3

### 3.3 Identity Preservation Loss

Aforementioned losses measure the difference between two pictures. However, faces may be very similar, yet depict different people (see Figure 8). This motivates the development of similarity measures that are specialized to faces and tuned to specifically judge similarity according to whether two faces depict the same person or not, while being insensitive to other factors, such as pose or emotion.

Suitable “identity preservation loss” functions for this type of task have been obtained by training models to enforce higher embedding similarity for intra-class samples of a face and larger embedding distance for cross-class samples of a face. A major example is the ArcFace model [51] which was designed for face recognition tasks. As the result, embeddings of the same face produced by this model will be close to each other, but far from embeddings of other faces. The loss for comparing two faces using this model is computed as  $\mathcal{L}_{id} = 1 - \langle R(x), R(y) \rangle$ , where  $R$  is the ArcFace model which produces embeddings,  $x, y$  are the face images and  $\langle \cdot, \cdot \rangle$  is the cosine similarity.

### 3.4 Fréchet Inception Distance FID

The Fréchet Inception Distance (FID) [52] is widely used to measure how well the distribution of images produced by the generator fits the distribution over the images used in training. The higher the score, the more different these distributions are. The FID method embeds each image from these two distributions into a 2048-dimensional vector using the InceptionV3 neural network [53]. Then, these two distributions of embedding vectors are compared using Wasserstein-2 distance.

The embedding step makes FID somewhat similar to LPIPS (see Chapter 3.2) because higher-level features are used for comparison, not RGB pixel information. Both approaches share the heuristics that the DNN that provides the embeddings, normally one trained for image recognition, can approximate relevant features within the human visual system [48], and, thereby, leads to scores that correlate well with human perceptual judgment of similarity. This expectation has borne out well, and a low FID score has emerged as a key indicator that the generator is creating

images that are difficult for humans to distinguish from the images used during training.

The FID metrics is mostly used for measuring the performance of the generator, rarely as a loss function. One of the complications of using it as a loss function is that it is too computationally heavy for iterative training over many epochs because a large number of images is necessary for measuring distributions in conjunction with computing covariance between all pairs of images as well as passing gradients through the InceptionV3 network for every image. However, computing FID only once to measure the perceptual quality of generated images by a trained generator is computationally feasible and therefore it is widely used in many works.

## 4 LATENT SPACES OF STYLEGAN

In the original GAN architectures, the latent code is fed into the generator and the output is the generated image. However, these codes were found to be highly entangled with regard to interpretable image feature and, therefore, difficult to use for controlling the image output. This insight led to the idea of first passing the codes through a deep mapping network, thereby allowing the architecture to learn a new, intermediate representation with properties better tailored to the structure of the image space. Together with the idea of injecting these newly created codes into each level of the generator pipeline (instead of only at the beginning) this triggered the series of StyleGAN architectures. In these architectures, further mapping networks are employed to transform the layer-wise injected codes into style variables that then control modulation of the activities passing through their respective layer (with computational details further evolved in the course of succeeding StyleGAN architectures, see Figures 4a-c). This allows StyleGANs to offer very flexible control of the generation of images, with each layer contributing modifications at a different level of resolution. As a result of their mapping scheme, the StyleGAN architectures have more than one innate latent space ( $\mathcal{Z}, \mathcal{W}, \mathcal{S}$ ). These spaces are illustrated in Figure 5. Moreover, to increase the expressive power of StyleGAN, it is common to work with extensions of these spaces



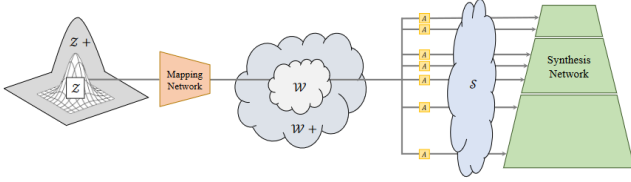


Figure 5: Latent spaces in StyleGAN [54].

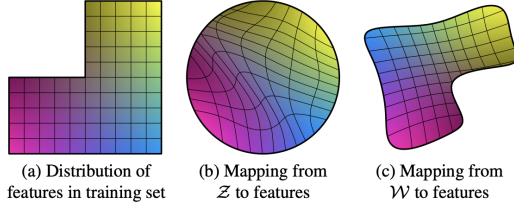


Figure 6: Disentanglement in the  $\mathcal{Z}$  and  $\mathcal{W}$  latent spaces [5]

( $\mathcal{Z}+$ ,  $\mathcal{W}+$ ). Here, we review the commonly used spaces and describe the differences between them.

#### 4.1 $\mathcal{Z}$ and $\mathcal{Z}+$ spaces

In the StyleGAN architectures, it accommodates 512-dimensional samples from an isotropic normal distribution with unit variance and zero mean which provide the random inputs  $z \in \mathcal{Z}$  at the root of the entire generation pipeline.  $\mathcal{Z}+$  space implies sequential mapping of  $18 z \in \mathcal{Z}$  vectors into 18 corresponding  $w \in \mathcal{W}$  vectors (relevant for StyleGAN and StyleGAN2 architectures with 18 layers).

#### 4.2 $\mathcal{W}$ space

Latent codes from  $\mathcal{Z}$  are transformed to latent codes in the 512-dimensional  $\mathcal{W}$  space of StyleGAN through the mapping network (see Figure 5). This transformation, which must be learnt during training, allows to distort the simple  $\mathcal{Z}$ -distribution into a distribution  $\mathcal{W}$  of the same dimensionality, but intended to be much closer to the required, usually very complex distribution of style parameters required to steer the generator pipeline to map the shared set of initial features in the first pipeline layer into richly structured distribution of natural looking face images. Figure 6 illustrates a (toy) situation where the feature distribution of to-be-generated images excludes a combination of two features, leading to a distribution where one quadrant of all possible combinations is absent (Figure 6(a), left). To create such a distribution from the disc-shaped input distribution  $\mathcal{Z}$  (Figure 6(b), middle) requires a very non-linear mapping. The eight fully connected mapping layers of the StyleGAN’s mapping network can provide the adaptivity to unfold the disc-shaped  $\mathcal{Z}$  space into a space  $\mathcal{W}$  whose shape is much closer to the required feature distribution (Figure 6(c), right). As a result, in this space meaningful editing operations on images can become realizable by simple axis-parallel movements of a point.

#### 4.3 $\mathcal{W}+$ space

Usually, a 512-dimensional vector  $w \in \mathcal{W}$  is used 18 times as the style input to 18 layers of the StyleGAN2 generator. This suggests that each of these 18 can be individually modified for fine-tuning of a generated image. This extends latent space into 18 copies of  $\mathcal{W}$  ( $d=18 \times 512$ ) and is denoted by  $\mathcal{W}+$  (see Figure 5). This larger space is able to provide a different latent code for each layer of the StyleGAN generator (e.g., 18 for a StyleGAN2 generator with a  $1024 \times 1024$  output resolution).

Since the StyleGAN architecture is trained using  $\mathcal{W}$  space, images sampled from  $\mathcal{W}+$  do not necessarily have realistic perceptual quality. This reflects the fact that operating in  $\mathcal{W}+$ , it is possible to reach areas that are outside the learned distribution of  $\mathcal{W}$ . This can allow to generate entirely novel patterns that are still face-like (e.g. “aliens”). However, it may also lead to patterns with useless structure or level of quality. As the distribution of  $\mathcal{W}$  cannot be explicitly modeled, keeping the latent code in within a range that corresponds to semantically and quality-wise useful patterns is a challenging task. To learn more about trade-offs between  $\mathcal{W}$  and  $\mathcal{W}+$  spaces see Chapter 5.2.3.

#### 4.4 $\mathcal{S}$ space

In a further step of StyleGAN processing, the latent code  $w \in \mathcal{W}$  of an image is further transformed to  $s \in \mathcal{S}$  vectors for each layer of the StyleGAN generators. The details of these transformations differ slightly between the versions, but a shared commonality is a mapping to a parameter vector of style parameters  $\mathcal{S}$  that parametrizes a set of affine transformation (one for each layer) that either normalize the activity pattern in a layer (in the case of StyleGAN), or that directly define a two-step scaling of the weights of a layer (mod/demod operations of StyleGAN2 and StyleGAN3). While the activity normalization in StyleGAN requires a specification of two parameters (bias and scaling) for each feature map, StyleGAN2/3 get by with a mere scaling (single parameter) for the feature map scalings in the mapping layers. In the interest of a compact presentation, we focus in the following only on the case of StyleGAN2 (which is very representative of the major ideas behind the style mapping) and refer the reader for the other two architectures to the original papers [5] [22].

At the style input of every layer of the StyleGAN2 generator is an independent single-layer perceptron (with identity activation function) denoted by  $A$  (affine transformation). This network maps  $w \in \mathcal{W}$  vector into a new vector  $s \in \mathcal{S}$  vector that provides for each of the layer’s weight kernel a separate scalar scaling parameter. The size of the vector  $s \in \mathcal{S}$  equals the number of channels in all layers of the StyleGAN2 generator. For example, in StyleGAN2  $\dim(\mathcal{W}) = 512$  and  $\dim(\mathcal{S}) = 9088$  [55]. This modulated kernel is then applied to the layer  $L - 1$  of StyleGAN2 generator to produce activation of the channel in the layer  $L$  of StyleGAN2. In [55] Wu et al. proposed to name this latent space of coefficients  $s$  StyleSpace  $\mathcal{S}$ . Analysis from Wu et al. indicates, that the  $\mathcal{S}$  space is more disentangled than previous latent spaces of StyleGAN2. The usecases of  $\mathcal{S}$  space for face editing is described in Chapters 6.1.3 and 6.1.4.

## 5 GAN INVERSION TO LATENT SPACES OF STYLEGAN

It is important to know the latent representation of an image of a face in StyleGAN space in order to manipulate that image or combine it with the style of some other image of a face. To find this representation is the task of *GAN inversion*.

Since a StyleGAN has several latent spaces (see Figure 5), this task can come in different variants, depending on the choice of the latent space for which a representation is sought. Furthermore, we shall see that these different choices may entail different properties, e.g. how the image will change under manipulations of its latent code, but also how well the inversion can be steered to faithfully capture the important visual features of the given real image. This chapter will discuss these, and further, main challenges of GAN inversion and review recently developed solutions in the form of inversion encoders that map an image to a suitable latent code.

After a brief overview over the major groups of inversion methods in general (Chapter 5.1) we turn in Chapter 5.2 to the important issue of *evaluating* the inversion, by suitable metrics, for distortion, perceptual quality, and editability, and how to control a suitable tradeoff between these properties. Achieving an approximate resemblance is relatively easy (see Figure 8), but resemblance in fine detail is very important for the perception of faces.

Then, in Chapter 5.3, we delve into specific methods for obtaining inversion encoders that can solve the inversion task: *pixel2style2pixel* (pSp) [56], *encoder4editing* (e4e) [57] and *ReStyle* [58]. Finally, Chapter 5.4 describes techniques for improving inversion quality for a subset of codes by selective tuning of StyleGAN generator weights: *Pivotal Tuning* [59] introduces optimization-based fine-tuning of StyleGAN; *MyStyle* [9] extends fine-tuning to hundreds of portrait images of a given person; *HyperStyle* [60] introduces encoder based prediction of fine-tuning weights of the StyleGAN generator.

### 5.1 Major groups of inversion methods

Inversion methods can typically be divided into three major groups of methods: *gradient-based optimisation* of the latent code (Chapter 5.1.1 and Figure 7A), *direct encoder-based mapping* onto the latent code (Chapter 5.1.2 and Figure 7B), and *fine-tuning* of weights of the StyleGAN generator (Chapter 5.1.3 and Figure 7C & D).

#### 5.1.1 Gradient-Based Optimization of the Latent Code

Gradient-based optimization methods (see Figure 7A) [7] [3] [61] directly optimize the latent vector using gradients from the loss between the real image and the generated one. Such methods can find a latent representation of the original image with a reasonable similarity (see Figure 8). However, there still exist three main drawbacks [7]:

- The optimization procedure is time-consuming, typically taking at least several minutes on a modern GPU.
- The final reconstruction image is sensitive to the choice of the random initialization.

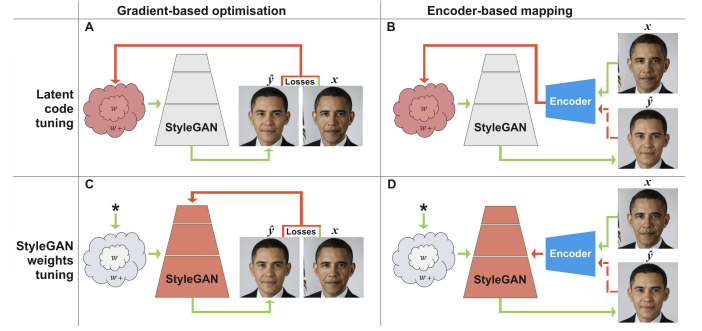


Figure 7: Inversion methods: target image  $x$ , reconstruction image  $\hat{y}$ , initial inversion  $*$ . Typical losses are  $L_2$ , LPIPS [48], ArcFace loss [51].

- The found latent point in  $\mathcal{W}$  or  $\mathcal{W}+$  spaces through inversion optimization steps is less stable while editing of the generated image than latent points obtained by sampling from  $\mathcal{Z}$  space and generating latent points in  $\mathcal{W}$  or  $\mathcal{W}+$  spaces through the mapping network (from  $\mathcal{Z}$  to  $\mathcal{W}$  space). The mapping network generates points in the distribution of the training dataset, while inversion optimization steps can move the latent point away from the distribution of the training dataset (see Chapter 5.2.1).

#### 5.1.2 Encoder-Based Mapping to the latent code

Alternatively, encoder-based methods for finding the latent code (see Figure 7B) [56] [57] train an encoder network over a large number of samples to directly map from the RGB image space into a latent space of StyleGAN. Once trained, the encoding can be done in the fraction of a second needed to process through the CNN encoder. Latent points obtained from the encoder network are more suitable for editing [57] by moving the point in the latent space, as the encoder network is trained to generate points inside the distribution of the training dataset of StyleGAN. However, training such an encoder is not trivial since it should be able to infer reasonable latent codes for a wide range of images beyond the training dataset. Thus the image generated from the obtained latent code found as the best match for a given real face image may have lost the identity of the original face (see Figure 8).

Conventional image- and feature-level losses (i.e. MSE and Perceptual losses [48] [64]) between the input image and the reconstructed image, may not be enough to guide the training of the encoder network. Wei et al. [65] proposed the method of training the encoder in cooperation with an optimisation-based iterator. One more possibility for getting a better inversion quality is to compute the loss based on SSIM [66], Identity loss [51] and LPIPS [48]) to train an encoder that maps RGB into  $\mathcal{W}$  space. An additional option is encoding into the  $\mathcal{W}+$  latent space that provides finer control over the generator, utilizing regularization methods while training of such RGB to  $\mathcal{W}+$  encoder [57].

#### 5.1.3 Fine-tuning of the StyleGAN generator

When an image of a face includes something outside the trainin distribution e.g., a tattoo or makeup (see Figure 12),



Figure 8: Obama [62] and Actress [63] before (upper row) and after Inversion (lower row). This inversion was performed using StyleGAN2-ada [4].

it is difficult to find a good inversion, as there is no such a point in the latent space of the StyleGAN generator that allows for reconstruction of such face-specific details. In this case, a possible solution is to fine-tune the StyleGAN generator weights themselves, using the target image or a set of target images. This motivates a set of methods that operate directly on the generator weights to improve the inversion quality of a given image.

Before starting such fine-tuning of the StyleGAN generator, the target image must be first inverted into StyleGAN’s latent space (see asterisk in Figure 7C&D) to the best possible reconstruction match using the previously discussed approaches (see Figure 7A&B). Then the StyleGAN generator model can be fine-tuned using loss-functions applied to the reconstructed and target images (see Figure 7C and Chapter 5.4.1).

Fine-tuning the StyleGAN generator by gradient-based optimization (Figure 7C) for each new image requires a couple of minutes of computation. This makes such methods difficult to apply in practice. By analogy with encoder-based methods for predicting the inversion latent vector (see Figure 7B), we can, here too, seek an encoder whose output is used to modulate the weights of the StyleGAN generator (Figure 7D). An example of such an approach is *Hypernetworks* [60]. The created *Hypernetwork* is trained to scale channel-weights of kernels of selected layers of the StyleGAN generator to match the target image and image generated by StyleGAN from the latent code (see Figure 7D and Chapter 5.4.3).

## 5.2 Evaluating GAN Inversions

### 5.2.1 Reconstruction quality vs. editability in StyleGAN

In addition to preserving similarity to the original image, the central motivation of the inversion step is to facilitate further latent editing operations. There exist a variety of points in the latent space that result in similar images to the original

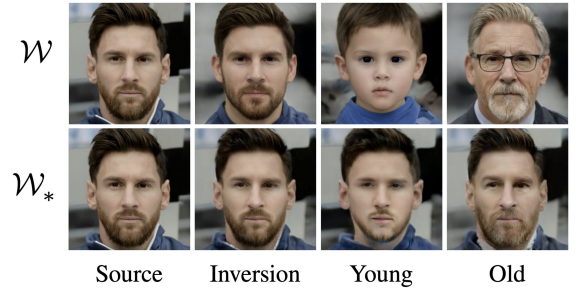


Figure 9: The editability gap in  $\mathcal{W}_*$  space. In paper [57] the space of vectors in  $\mathcal{W}$  that are out of the mapping network manifold was denoted as  $\mathcal{W}_*$ .

one, some of these points are more suitable for latent editing than others [57] [67] [68]. A successful encoding of a real image into a latent space should enable decent editability via the latent code.

### 5.2.2 Distortion, perceptual quality, editability

Following the above observations, inversion methods and reconstruction quality should be evaluated based on several components: **distortion**, **perceptual quality** and **editability**. Simply put, **distortion** is a dissimilarity between the reconstructed image and the original image (e.g. MSE, SSIM, LPIPS) between the original and reconstructed images [47]. Distortion alone, however, does not capture the quality of the reconstruction. **Perceptual quality** measures how realistic the reconstructed images are (e.g. adversarial discriminator), with no relation to any reference image [47]. **Editability** stands for maintaining high perceptual quality of the image generated from the *edited* latent code [57]. The work [47] proved that there exists an explicit trade-off between distortion and perceptual quality. Therefore, both the distortion and the perceptual quality of the reconstructed images must be evaluated to provide a complete evaluation of inversion method. It is desirable that we can find a latent point for a given image with good edibility and reconstruction quality.

### 5.2.3 Distortion vs. perceptual quality and editability trade-off

All possible output vectors of the StyleGAN mapping network constitute its latent space  $\mathcal{W}$ , where the input vectors of the mapping network are normally distributed vectors in  $\mathcal{Z}$  space. Latent vectors generated as the result of an inversion method may, however, not necessarily lie within this manifold of the StyleGAN mapping network  $\mathcal{W}$ . In [57] and Figure 9 the set of such vectors is denoted as  $\mathcal{W}_*$ . Moreover, manipulation via the inverted image code can be performed not only in  $\mathcal{W}$  or  $\mathcal{W}_*$  latent spaces of StyleGAN, but also in  $\mathcal{W}+$  space, where vectors for 18 layers of StyleGAN2 are independent but each 512-dim style vector belongs to  $\mathcal{W}$  space.

These options for choosing a representation space have been found to differ in interesting ways: In  $\mathcal{W}$  space, reconstructions have the highest distortion, but good editability and perceptual quality. In  $\mathcal{W}_*$  space (see Figure 9), reconstructions have the lowest distortion, but the worst editability and perceptual quality after editing. In  $\mathcal{W}+$



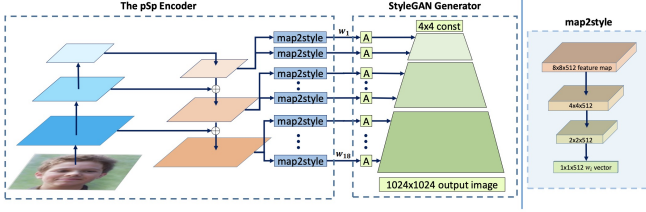


Figure 10: pSp encoder architecture [56].

space, reconstructions have low distortion, good editability and perceptual quality.

### 5.3 Inversion Encoders

Inversion encoders solve the GAN inversion task in the form of a direct mapping from an image onto a latent code. Therefore, and ideally, the concatenation of the GAN and the Inversion Encoder should produce the identity mapping. An early version of this idea came up in BiGAN [69], where the forward and backward mappings are developed simultaneously. However, with regard to StyleGAN inversion, the inverted part of the GAN is not the entire path from the image to its  $z$ -input, but to one (or several) of its intermediate latent spaces (see Chapter 4).

#### 5.3.1 pSp Encoder: Image-to-StyleGAN

The idea behind the *pixel2style2pixel* (pSp) inversion encoder into  $\mathcal{W}+$  space [56] is based on the fact that different layers of the StyleGAN architecture correspond to different levels of generated detail (coarse, medium, and fine). Similarly, different layers of CNN-encoder feature maps also correspond to different levels of detail (coarse, medium, and fine). In the pSp encoder (see Figure 10) feature maps are first extracted using a standard feature pyramid over a ResNet backbone. For each of the 18 target styles, a small mapping network is trained to extract the learned styles from the corresponding feature map, where styles (0-2) are generated from the small feature map, (3-6) from the medium feature map, and (7-18) from the largest feature map. The mapping networks, *map2style*, are small fully convolutional networks, each of which generates a 512  $\Delta_i$  vector that are added to  $\bar{w}$ , where  $\bar{w}$  is the mean of the distribution of the *mapping network* output vectors when sampling in  $\mathcal{Z}$  space [56]. The resulting  $18 \times 512$  vectors  $\bar{w} + \Delta_i$  in the  $\mathcal{W}+$  space are fed into the StyleGAN, starting from its matching affine transformation,  $A$  (see Figure 10) [56]. The pSp encoder is trained using the following loss functions:  $L_2$ , LPIPS [48], Identity [51] and additional regularization loss. For the training of the encoders the weights of the StyleGAN generator are frozen, leaving as the adapted components only the ResNet backbone, the upsampling layers, and the *map2style* mapping networks.

#### 5.3.2 e4e Encoder for StyleGAN Image Manipulation

Motivated by the goal to find a “golden mean” in the previously described distortion-editability tradeoff (see chapter 5.2.1), the authors of [57] analyse the structure of the StyleGAN latent space and the innate trade-offs between distortion, perceptual quality and editability to take the pSp

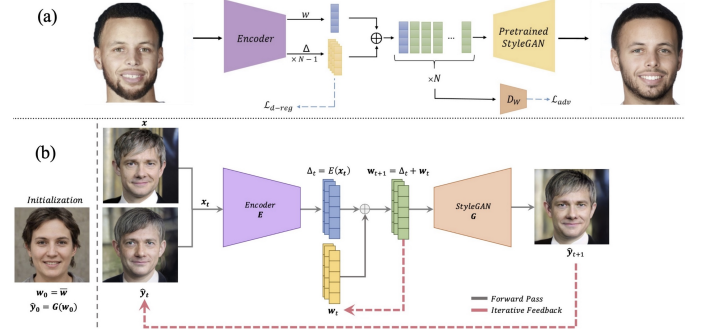


Figure 11: (a) e4e encoder architecture with “progressive” training of encoder sequence by combining regularization, adversarial and distortion losses (not depicted) to improved control of editability-distortion tradeoff [57]. (b) *ReStyle* iterative inversion scheme [58].

approach further and propose a novel encoding scheme. Hereinafter this method will be called *encoder4editing* or simply *e4e* (Figure 11a). Their starting point is the above described pSp architecture [56] (Figure 10), i.e., the encoder’s input is an image and the encoder output is a tensor of shape  $18 \times 512$  in the  $\mathcal{W}+$  space, whose first  $1 \times 512$  values specifies the StyleGAN2’s  $w$  vector, and its remaining  $17 \times 512$  values represent the  $\Delta_i$  vectors for the last 17 layers of the StyleGAN2 generator. Now, instead of training all components of this tensor simultaneously, the authors propose a “progressive” learning scheme that they structure in the following way: first, learning starts with setting all  $17 \times 512$   $\Delta_i = 0$ , thus training only the first  $1 \times 512$  values for matching StyleGAN2  $w$  vector. Subsequently, the mapping networks sequentially unfreeze learning of their  $\Delta_i$  outputs for the higher layers  $i = 2 \dots 18$  of the StyleGAN2, in ascending order. This scheme allows the encoder to first learn a coarse reconstruction, to which it then learns to add increasingly finer details.

Additionally, they propose a refined regularization scheme for the  $17 \times 512$   $\Delta_i$  vectors to keep  $w + \Delta_i$  in the space  $\mathcal{W}$  to achieve a better editability, due to the individual adjustment of the style vector  $w$  for each layer of generator, along with improved perceptual quality. This regularization scheme employs three parts: a  $L_2$  regularization loss is used to minimize the joint variance of all  $\Delta_i$  ( $\mathcal{L}_{d-reg}$  in figure 11a). A second part is a loss derived from a latent discriminator ( $\mathcal{L}_{adv}$  in figure 11a) which is trained in an adversarial manner to discriminate between latent codes from the “true”  $\mathcal{W}$  (obtained by feeding samples from  $\mathcal{Z}$  to the StyleGAN encoder), and the encoder’s learned latent codes. Finally, to make the  $\Delta_i$  also to contribute to distortion reduction, additional distortion losses ( $L_2$ , LPIPS [48], and Identity preservation ArcFace [51]) are added.

#### 5.3.3 ReStyle: Iterative Inversion Refinement

The authors of [58] introduced a further idea to the previously discussed methods [57] [56]. Unlike typical encoder-based inversion methods that infer the input’s inverted latent code using a single forward pass, their *ReStyle* method adds an iterative inversion mechanism with an additional feedback input (see Figure 11b). This can be seen as introducing another level of “progressive” processing, this time

not for sequential structuring of learning, but instead for the encoding operation itself. Specifically, the inversion is performed using several forward passes by feeding the encoder with the output of the previous iteration, always paired with the original input image. This allows the encoder to leverage results from the previous iterations to highlight the relevant regions needed for achieving an accurate reconstruction of the input image.

Given a source image  $x$  and its initial reconstruction  $\hat{y}_0 = G(w_0)$  from the initial representation  $w_0 = \bar{w}$  set to the average style of the generator, this method performs  $N > 1$  steps to predict a sequence  $w_t, t = 1..N$  of the image style codes, with the final inversion  $w = w_N$  and its associated reconstruction  $y = G(w)$  as the final results. At each step  $t$ , the encoder  $E$  receives an input  $x_t = (x, \hat{y}_t)$  consisting of the original image  $x$ , paired with its reconstruction  $\hat{y}_t$  from the most recent time step, to compute a refined new “residual” code  $\Delta_t = E(x_t)$ , which is added to the inversion code of the source image as  $w_{t+1} = \Delta_t + w_t$ . The new latent  $w_{t+1}$  is passed again through the StyleGAN generator to update image reconstruction  $\hat{y}_{t+1} = G(w_{t+1})$ , which is used in the next iteration. This procedure is initialized with the StyleGAN generator’s average style vector and its corresponding synthesized image, respectively.

The *ReStyle* approach demonstrates better  $L_2$ , LPIPS [48], and Identity [51]) metrics than encoder-based approaches [57] [56] when we increase the number of iterations, but inference time is still less than inference time of gradient-optimization-based methods. Therefore, this method can be seen as a favorable compromise between encoder-based and gradient-optimization-based methods, regarding reconstruction quality as a function of inference time.

## 5.4 Fine-tuning of the StyleGAN generator for better inversion

Images of real faces often contain various unique details such as tattoos, scars, fashion elements or light. It is challenging to apply identity-preserved editing to such out-of-domain face images even with the previous methods. Inversion of such face images may lead too far away from the generator’s domain, because the nearest image in this domain may not have these all details. As a result they will be lost after the editing process (see Figure 12).

### 5.4.1 Pivotal Tuning for Latent-based Editing of Real Images

To better cope with the inversion problem of unique face details (e.g., tattoos) the paper *Pivotal Tuning* [59] proposes to use an initial inverted code as a “pivot” around which the StyleGAN generator is fine-tuned, rather than trying to solve the problem by focusing on improving search for a proper latent code alone.

The method inverts the source image  $x$  to style code  $w_p \in \mathcal{W}$  in the native latent space of StyleGAN, which will be called as the pivot code. The inversion step is a gradient based optimization of source image reconstruction using LPIPS,  $L_2$  losses and noise regularization. However, mapping this pivot code produces only an image that is similar to the original one, but may exhibit significant distortion as explained before (see Figure 12).



Figure 12: Comparison of *Pivotal Tuning* [59] and other inversion methods (see [3] [7] [59], and Chapter 5.3.2))

To remedy this, the method adds a tuning step for the StyleGAN generator. Let  $x^p = G(w_p; \theta)$  be the image generated from the pivot code  $w_p$  when using the generator with weights  $\theta$ . The tuning step then consists of adapting the weights between the pivot code and the output to bring  $x^p$  closer to  $x$  using LPIPS and  $L_2$  losses. The mapping network layers between  $z$  and  $w$  remain frozen.

However, it is important to constrain the changes of the tuning such that they only affect the reconstruction mapping within a neighborhood of the pivot code  $w_p$ . To achieve this, they introduce a suitably designed regularization term, implemented in the form of an iterative process. At each iteration, a  $z$  value is sampled from the standard normal distribution and the StyleGAN mapping network produces corresponding style code  $w_z$ . The difference  $w_z - w_p$  and  $w_p$  gives a direction away from the pivot point whose length is scaled to the value of a coefficient  $\alpha$ . The resulting end point  $w_r$  of this scaled vector, attached to the pivot point  $w_p$  (see equation 1) is a code in a certain neighborhood of the pivot  $w_p$ :

$$w_r = w_p + \alpha \frac{w_z - w_p}{\|w_z - w_p\|_2}. \quad (1)$$

It contributes a regularization step for the fine-tuned StyleGAN generator by adapting the weights  $\theta^*$  of the latter towards minimizing the distance between the image pair  $(x_r, x_r^*)$  obtained from  $w_r$  with original generator ( $x_r = G(w_r, \theta)$ ) and the tuned generator ( $x_r^* = G(w_r, \theta^*)$ ), using LPIPS and  $L_2$  loss functions. This neighborhood-restricted tuning process ends up altering appearance features that represent mostly face identity, without interfering with editing capabilities.

### 5.4.2 MyStyle: A Personalized Generative Prior

The MyStyle architecture [70] [9] extends the idea of pivotal fine-tuning from a single to hundreds of pivots, all taken to be portrait images (called “anchors”) of a given person. This allows it to use the StyleGAN2 generator as backbone for super-resolution (see Chapter 8.3), inpainting or semantic editing tasks. For the required, now multiple-anchor, fine-tuning it uses LPIPS [48] and  $L_2$  pixel losses. The authors propose to collect about 100 anchor examples of known pictures of a person that form a “personalized region” in the latent space  $\mathcal{W}$  of the StyleGAN2 generator. It takes about 80 minutes to fine-tune a StyleGAN2 generator on 100 portrait image examples on a single GPU.

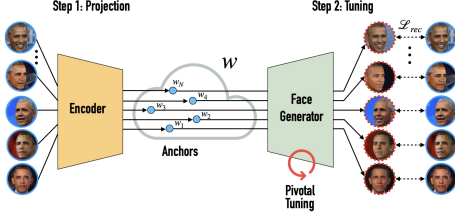


Figure 13: *MyStyle* fine-tuning scheme of the StyleGAN generator [9] using pivotal tuning around a large number of anchors given by a collection of views of the face of a single person.

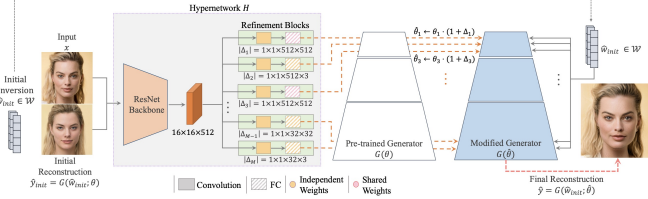


Figure 14: HyperStyle method illustration [60]

The anchor space of example images for fine-tuning is used to get personalized results. This space was described by Generalized Barycentric coordinates, which allows us to detect when a latent point is inside the convex region of known anchors in the latent space, and when a latent point is outside this region. Let  $\mathcal{A}$  be the space of Generalized Barycentric coefficients. Then any point inside this personalized region is described by a linear combination of anchor vectors in this alpha-space of coefficients.

For semantic editing task is necessary to preserve personality. Existing directions in the latent space are learned for the whole domain of faces and are not personalized. Because of this, some directions may lie outside the anchor space and any small step in this direction will lead to degradation of the quality of the edited image. To solve this problem we need to project the direction on the alpha space and perform editing in it. This operation will transform an infinite linear editing to one with endpoints. Even if the direction is in anchor space, this space can limit the movement of the latent point, resulting in poor editing quality. This problem can be solved by using the beta-dilation parameter, which shows how far the latent code can go beyond the boundary of the anchor space. This makes it possible to get more editable images with an adjustable loss of personality.

#### 5.4.3 HyperStyle: StyleGAN Inversion with HyperNetworks for Real Image Editing

The *HyperStyle* [60] approach proposes to combine several ideas of the previous discussed approaches of *ReStyle* [58] (iterative improvement with inversion encoder), *Pivotal Tuning* [59] (fine-tuning of StyleGAN generator weights for a specific image of a face), and *e4e* [57] (initial inversion prediction of  $w \in \mathcal{W}$ ) for fine-tuning the pre-trained StyleGAN generator on the fly.

Key idea is to learn to predict coefficients for a channel-wise scaling of weights of selected layers of the pre-trained

StyleGAN generator (see Figure 14) to personalize it for a given image of a face. In this way *HyperStyle* is computationally much lighter direct mapping for fine-tuning coefficients of the StyleGAN generator, than the gradient based fine-tuning approaches like *Pivotal Tuning* [59]. The required scaling of channel weights is parametrized as  $\hat{\theta}_l^{i,j} := \theta_l^{i,j} (1 + \Delta_l^{i,j})$ , where  $\theta_l^{i,j}$  denotes the weights of the  $j$ -th channel in the  $i$ -th filter in the StyleGAN generator's  $l$ -th layer and  $\Delta_l^{i,j}$  is the output of the Refinement Blocks (see Figure 14). For a better trade-off between network expressiveness and feasibility of learning, the *HyperStyle* model is trained to predict scaling coefficients not for all kernels, but only for kernels of selected StyleGAN generator layers. As the initial inversion capture coarse details, only layers that are responsible for medium and fine details may be selected.

The *HyperStyle* architecture with iterative refinement of StyleGAN weights (depicted in Figure 14) consists of a *ResNet* backbone that receives a source image with its initial reconstruction and Refinement Blocks of convolutions and fully-connected layer. Training is guided by an image-space reconstruction objective through pixel-wise  $L_2$ , LPIPS [48] and ArcFace [51] losses.

## 6 EDITING FACE IMAGES WITH STYLEGAN

The main idea about editing of an image using StyleGAN is that editing is achieved through some manipulation of its latent code, thereby moving the point that represents this latent code within one of the latent spaces of StyleGAN (see Chapter 4). At first we do not know how movement in the latent space will affect the generated image but there are methods to learn how to navigate the latent Space to edit an image in a more controlled and semantically meaningful manner. Movement of the point in a wrong or a random direction will in the worst case lead away from the face distribution (thereby destroying the "faceness" of the image), or lead to an undesired, simultaneous change of different attributes, most likely accompanied by a loss of identity of a person on the image.

In this chapter we will focus on methods to identify directions in a latent space of StyleGAN which are correlated with desired, *semantically interpretable editing attributes*, like smile, pose, hairstyle, age, and so on. Also, we will discuss how the different latent spaces of the StyleGAN architecture differ with regard to their editing properties.

Identifying semantic directions can typically be divided into global semantic directions (see Chapter 6.1) and single image semantic directions (see Chapter 6.2). Chapter 6.1.1 introduces a supervised approach for finding semantic directions by means of hyperplanes between points with and without chosen attributes. Chapter 6.1.2 offers an unsupervised approach for discovering semantic directions by using PCA. Chapter 6.1.3 describes discovering directions in StyleSpace using only few points with known attributes. Chapter 6.2.1 introduces a text-driven approach for discovering semantic directions.

### 6.1 Global semantic directions

The first class of approaches is based on averaging a direction in latent space correlated with the given attribute over





Figure 15: Moving along the 10th principal component in 7-8 layers changes hair color [72].

a number of contrastive pairs, with and without a desired attribute.

### 6.1.1 Identifying Semantic Directions in a $\mathcal{W}$ space of StyleGAN

InterFaceGAN [71] belongs to the first editing class and proposes a supervised method for identifying semantic directions in a StyleGAN’s latent space and then using these directions for face editing.

Suppose there is a pretrained binary classifier for some attribute we want to edit. We make an assumption that for any binary semantic attribute there exists a hyperplane in the StyleGAN latent space serving as the separation boundary between points of positive and negative examples of that attribute. To find a suitable separating hyperplane that represents editing direction in the latent space  $\mathcal{W}$  of the StyleGAN, the authors of [71] propose to apply a linear SVM to points of positive and negative examples of the selected semantic attribute. To identify points of positive and negative examples in the StyleGAN latent space  $\mathcal{W}$ , they generate images for 500,000 randomly selected latent points and use the scores of a pretrained ResNet binary classifier to identify a subset of 10,000 images for which the classifier reports the highest scores (attribute is present), and 10,000 image with the lowest scores (attribute is absent). To manipulate the attribute of an image, we move the original latent point along the normal vector of the hyperplane.

When we edit several of fine-grained attributes, one may affect another. To achieve a more disentangled editing it was proposed to orthogonalize a discovered set of semantic directions [71]. For example, given two hyperplanes for two semantics with normal vectors  $n_1, n_2$ . Then we can find a projected direction  $n = n_1 - (n_1^T n_2) n_2$  such that editing along this projected direction correlates with the first attribute, but is not affecting the second attribute.

### 6.1.2 Discovering Interpretable Semantic Directions in $\mathcal{W}$ space

In contrast to the previous, supervised method, GANSpace [72] describes an unsupervised approach for discovering semantic directions. The method, which requires only a pretrained StyleGAN generator, proposes sampling of a large number of random points in  $\mathcal{Z}$  space, collecting the corresponding points in  $\mathcal{W}$  space, and applying PCA to obtain a basis in  $\mathcal{W}$  space. These PCA basis vectors contain the semantic directions responsible for some attributes.

Within their study, using on the order of 100 basis vectors, the authors find that large-scale changes to geometric configuration seem to be limited to the first 20 principal components. For a further refined control of editing features, these PCA directions can be applied individually to each of the 18 StyleGAN2 layers. By checking the influence of the discovered PCA directions, it is possible to identify directions responsible for specific face editing attributes, for example hair color (see Figure 15). The authors show that such a check – in their work of about 1800 combinations – can be done both automatic or manual.

### 6.1.3 Identifying Semantic Directions in StyleSpace of StyleGAN

The search for semantic directions can be done not only in the  $\mathcal{W}$  space, but also in the more disentangled StyleSpace ( $\mathcal{S}$  space, see Chapter 4.4) [55]. In this space, identification of semantic directions can already succeed with as few as 10 to 30 positive examples that contain the target attribute. This utilizes the idea that the differences between the mean style vector of the positive examples and the mean of the entire generated distribution of 500k samples in  $\mathcal{S}$  space reveal which StyleGAN channels are the most relevant for the target attribute [55]. Such channels can be identified, e.g., with statistical methods that determine which vector components show statistically significant deviations towards higher values. Once we know the right channel, we can change its activation along the corresponding  $\mathcal{S}$  dimension so that the generated image shows an increase or decrease of the desired semantic attribute.

### 6.1.4 Text-Driven Discovering of Global Semantic Directions by CLIP

It is also possible to search for a global semantic direction by creating combined image-text embeddings, as in the CLIP [23] [6] model. Here, the key idea is to assume that direction vectors are parallel for CLIP text and CLIP image embeddings. We then can take the direction between text embedding vectors such as “face with smile” and “face” in the latent space of CLIP as the “smile” semantic direction in that space. This resembles the first class of global semantic editing approaches that we discussed in Chapter 6.1).

To harness this idea for finding the global direction of an example attribute “smile” in the StyleSpace  $\mathcal{S}$ , for some image, we move the coordinates of its point in the positive and negative directions for a selected channel (by the value of the standard deviation ( $\sigma$ ) in that channel multiplied by a perturbation magnitude). This will produce a pair of generated images ( $\pm\sigma$ ) that can be fed into CLIP to measure how the perturbed direction of the chosen StyleGAN channel in original  $\mathcal{S}$  space is correlated with changing the association of the text attribute “smile” to the image pair by CLIP. Instead of relying on a singly, possibly noisy, sample, this process is repeated for a modest number of images (e.g.  $N = 100$ , always using the same channel in  $\mathcal{S}$  space) to compute the corresponding averaged direction in CLIP space. Its projection on the “smile” text attribute then provides a direct measure (with reduced variance as compared to a single sample) how much the chosen channel in  $\mathcal{S}$  space affects the obtaining of the paired text (here: “smile”). After going through all the StyleGAN2 channels,

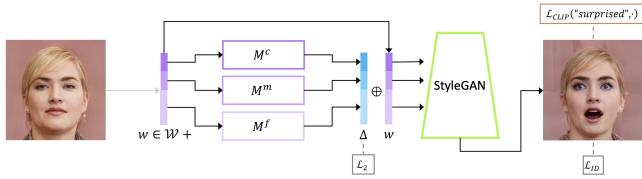


Figure 16: *StyleCLIP* mapping network architecture [6]. For a fixed “surprised” text attribute three mapping networks  $M^c$ ,  $M^m$  and  $M^f$  for coarse, medium and fine scale are trained for images to map their latent vector  $w$  (blue bar, left) of images into a short change direction  $\Delta$  that, if added to  $w$  (blue bars, right side), moves the generated output towards better satisfying (lower CLIP loss of the new image-text pair) the chosen text attribute.

we select those with projection values greater than a certain threshold. Finally, we obtain the text attribute direction in the  $\mathcal{S}$  space as given by these StyleSpace  $\mathcal{S}$  channels with their projection values.

## 6.2 Single image semantic directions

The second class of approaches optimizes a single image and requires an assessment network over the generated image, like CLIP or a binary attribute classifier. Loss from such an assessment network produces a gradient step in latent spaces which indicates the direction to move the input point of the generator to decrease the target attribute loss.

### 6.2.1 Text-Driven Manipulation of StyleGAN Imagery by CLIP

The *StyleCLIP* [6] offers a text-based approach to image editing. It is again based on the CLIP architecture [23] (already considered in 6.1.4), making use of CLIP’s combined latent space for text-encoder and image-encoder. CLIP’s text-encoder produces the embedding of the attribute text and the CLIP’s image-encoder produces the embedding of the StyleGAN generated image. The CLIP-model produces gradients through the CLIP image-encoder to minimize the similarity loss of text and image points in the combined latent space of CLIP. Connecting CLIP to the image output of the StyleGAN thus allows to obtain the overall gradient that indicates the editing direction for the point in the  $\mathcal{W}$  latent space of StyleGAN with regard to any textual attribute that is represented in CLIP. In addition, Identity [51] and  $L_2$  losses on the StyleGAN generated image allow to penalize losing the person’s identity in the generated image under text-attribute driven changes. However, the disadvantage of this method is the need to conduct computationally expensive gradient based optimization steps for each image and text attribute, because each pairing of image and text attribute gets its own editing direction in a StyleGAN latent space.

As seen several times before, this problem of computationally expensive gradient based optimization can again be remedied by training an additional mapping network (Figure 16). Each text attribute that is of interest for editing, e.g. “smile”, requires to train a separate mapping network. This *StyleCLIP* mapping network [6] moves the point in  $\mathcal{W}+$  space according to the text attribute. The *StyleCLIP* mapping



Dog  $\rightarrow$  Nicolas Cage

Figure 17: StyleGAN-NADA [12] allows to create images that do not even exist in real life (“Nicolas Cage Dogs” using a generator trained to generate dogs and the “Nicolas Cage” text prompt).

network employs an architecture with three prediction sub-networks (denoted as  $M^c$ ,  $M^m$  and  $M^f$  in Figure 16) for the coarse, medium and fine layers of the StyleGAN2 generator respectively. Each sub-network takes the corresponding  $\mathcal{W}+$  dimensions as input and predicts  $\Delta_w$  for them (see Figure 16). The overall gradient guidance by the CLIP loss of the text-image pair is supplemented by terms to keep the result image in the vicinity of the input image (small  $L_2$  loss) and to preserve identity (identity loss  $L_{id}$ ). Authors employ the CelebA-HQ dataset [41] for training.

### 6.2.2 Interpretable Control: Facial Pose and Expression Change Based on FaceRig

To be able to create editable faces as flawlessly as possible, controlling semantic face parameters that are interpretable in 3D like face pose and expressions play a crucial role. StyleRig [13] by Tewari et al. offers nice results using both three-dimensional morphable face models (3DMM) in combination with StyleGAN to provide such control. (See Figure 1K for StyleRig examples)

## 7 CROSS DOMAIN FACE STYLIZATION WITH STYLEGAN

The original StyleGAN architecture allows mixing styles of two sources of information (see Figure 3) from the same training domain, for example CelebA-HQ dataset [41]. However, what if we want to mix styles of two sources of information from different domains, for example CelebA-HQ (Fig. 3) and cartoon faces (Fig. 22)? This chapter discusses approaches for style mixing from different domains by finetuning or merging the StyleGAN generators.

StyleGAN-NADA [12] proposes finetuning of the StyleGAN generator towards a target style domain using CLIP (see Chapter 7.1). The layer-swapping approach [73] devises a controllable domain adaptation between two different StyleGAN models (see Chapter 7.2). BlendGAN [74] proposes a style encoder for finetuning face StyleGAN such that its output becomes adaptable to an arbitrary style (see Chapter 7.3). StyleCariGAN [24] introduced shape exaggeration blocks to capture shape adaptation in caricature generation (see Chapter 7.4).

### 7.1 CLIP-Guided Domain Adaptation of StyleGAN

StyleGAN-NADA [12] allows to fine-tune the StyleGAN generator using CLIP based gradients towards a different



Figure 18: Layer swapping process. [73]

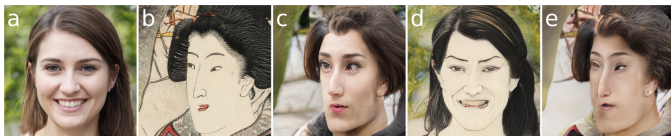


Figure 19: [73] (a) and (b) are samples of the "Base" and "Transferred" trained models, respectively. (c)(d)(e) are "Interpolated" results of different combination of layers from the "Base" and "Transferred" models.

style domain for example zombie faces. For that, first the zombie semantic direction is identified in CLIP latent space by subtracting embeddings of two text prompts "zombie face" and "face". Using the CelebA-HQ dataset [41] for training, the authors demonstrate that the semantic direction in CLIP latent space can be used to fine-tune a StyleGAN model [41] towards zombie generation. To this end, thousands of images of faces are generated by sampling a latent space of the trained StyleGAN model. Then, according to the loss, embeddings of these images in CLIP space have to move in a parallel direction to the found zombie semantic direction in CLIP text space. This parallel movement of thousands of points in the CLIP latent space becomes the training objective for changes of the StyleGAN model weights.

To solve overfitting and divergence problems, [12] proposes to fine-tune only StyleGAN layers which the most influence on the new domain and freeze weights of the rest of the layers. To determine finetuned layers, the approach moves these latent image points in CLIP space to the text embedding of the target domain and chooses those layers in which the latent code has changed the most. These layers are considered as sensitive to the new domain. Further only these layers are unfrozen and generator weights are fine-tuned by above mentioned method.

## 7.2 Layer Swapping for Controllable Domain Adaptation

Paper [73] proposed a cross domain face stylization approach for two given datasets. Suppose we have a "Base" StyleGAN2 model trained on a source dataset of faces (see Figure 19a). Then we make a copy of this trained StyleGAN2 model and continue training this "Transferred" copy on a target dataset like artistic portraits (see Figure 19b). Both StyleGAN2 models have the same mapping network. Then, the domain adaptation is done by creating a third "Interpolated" StyleGAN2 model by combining selected layers (see Figure 18) from the "Base" and "Transferred" models. Trying different combinations of layers allows to generate images with various generative characteristics (see Figure 19c,d,e).

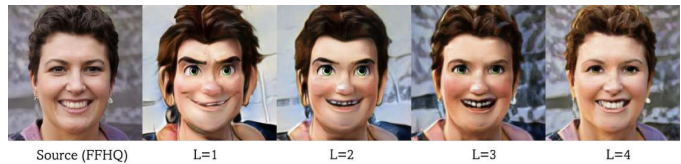


Figure 20: Effects of the number of swapped layers [75].



Figure 21: Examples of reference-guided BlendGAN synthesis [74].

Paper [75] managed to obtain remarkable results transforming images of human faces into cartooned images (see Figure 20). The approach also utilizes the layer swapping technique together with an additional structure loss while fine-tuning. Structure loss is calculated as MSE between extracted RGB outputs of each low-resolution block of the source and target generator.

## 7.3 Blending for Stylized Face Generation

Paper [74] suggested an alternative to the layer swapping mechanism (see Chapter 7.2). It proposed to train a StyleGAN model on an original dataset of faces, and fine-tune it on a second dataset of faces in different artistic styles (see Figure 21). A separate encoder is trained using contrastive learning on augmented variations of stylized images of faces. The encoder is trained to produce the same latent vector for geometric augmentations of the same style image, but distinct to latent vectors of other style images. Thus, the encoder becomes insensitive for facial details, but focused on the style of an artistic face image. The latent space of this encoder is connected to the latent space  $\mathcal{W}$  of StyleGAN via a second mapping network of 8 fully connected layers. The blending procedure is similar to the vanilla StyleGAN merging of two sources of information. The example is generated by taking a face domain latent code for some first layers and a style domain latent code for the other layers.

## 7.4 Caricature Generation via StyleGAN Feature Map Modulation

In the case of caricatures, the shape variations between the photo domain and the caricature domain are too large to successfully capture the exaggerations and color stylization of caricatures using the layer swapping technique (see Chapter 7.2). Therefore, StyleCariGAN [24] proposes to exaggerate the face shape features on the fly directly in the StyleGAN layers. To this end, StyleCariGAN introduces shape exaggeration (see Figure 22) residual blocks



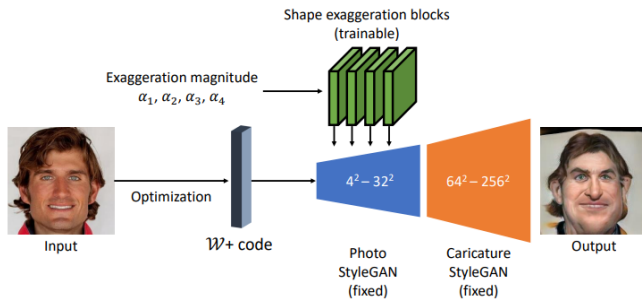


Figure 22: Architecture of the StyleCariGAN [24], using the first few resolution blocks of the photo-realistic StyleGAN and the last few resolution blocks of the caricature StyleGAN.

appended to the layers of the first four resolution blocks. They compute desirable feature map changes, which are then added to the original feature maps. Layers of the first four resolution blocks ( $4 \times 4$ ,  $8 \times 8$ ,  $16 \times 16$ ,  $32 \times 32$ ) of the photo StyleGAN and the last three resolution blocks ( $64 \times 64$ ,  $128 \times 128$ ,  $256 \times 256$ ) of the caricature StyleGAN are used for the photo-to-caricature StyleGAN (see Figure 22). Experiments with the StyleGAN model indicate, that the first four resolution blocks of the photo StyleGAN determine the structural information of the output, while the last three resolution blocks of the caricature StyleGAN determine the color styles for the caricature. In order to train these exaggeration blocks, [24] designed an adversarial loss, cycle losses, and an attribute loss.

## 8 FACE RESTORATION WITH STYLEGAN

Face restoration aims at recovering high-quality (HQ) face detail from low-quality (LQ) counterparts suffering from unknown degradation, such as low resolution, blur, compression artefacts or noise. Context information may allow to properly infer such missing detail. For example, location of hairs on a blurry face can be estimated from low resolution details of a face. Exact location of each hair is not important for human perception, but it is important to restore overall structure and texture. Thus one may expect that supervised training of neural network architectures with LQ-HQ training pairs using pixel-wise losses will not lead to high perceptual quality. Instead, pixel-wise loss functions cause over-smoothed result images, as the model tends to be the mean of high-quality faces.

However, architectures with energy-based components, like GAN discriminators, can be a good approach for reconstruction of fine detail from low resolution images and may provide perceptually plausible results. In the fully converged state, the discriminator will not be able to differentiate between a generated sample and a sample from the dataset. Ideally, the same will then also apply to human perception. Thus, we can expect GANs to be able to generate deblurred images of perceptually high-quality, but there remains the challenge of mapping a blurred input into an appropriate latent vector of StyleGAN that makes the StyleGAN to generate the corresponding deblurred version.

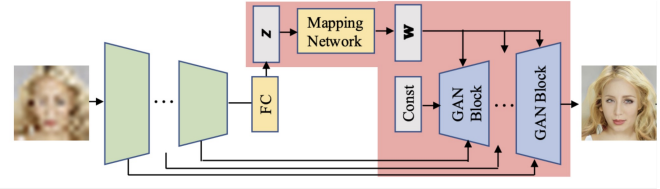


Figure 23: GPEN architecture [76]. A CNN encoder network receives a LQ input (left) and has learnt to provide  $z$ -input and via skip connections control inputs to additional input fields in the GAN generator layer hierarchy (right) to cause generation of a corresponding HQ output image.

### 8.1 GAN Prior Embedded Network for Blind Face Restoration in the Wild

The GAN Prior Embedded Network (GPEN) [76] is one of the solutions for blind face restoration problem. The main idea of this approach is to embed a StyleGAN like architecture as the decoder part into an encoder-decoder architecture, thereby utilizing its strong prior for generating high-quality faces. The LQ image is fed to the encoder part, which is realized as a conventional CNN whose output serves as the latent code for the subsequent GAN decoder to generate an appropriate HQ image (see Figure 23). To this end, the activations of the final CNN output layer are fed in place of the random vector into the GAN's latent space mapping network. Furthermore, to make efficient use of the controllability of the StyleGAN decoder, the GAN is slightly modified by padding its generator layers with additional input fields for receiving via skip connections activity patterns from more shallow layers in the encoder (see Figure 23). They are chosen such that the feature map hierarchy of the encoder CNN and the GAN generator layers become connected at matching levels of resolution.

In the first phase the GAN network (for example the StyleGAN generator) is trained to generate high quality faces from scratch. This phase uses the FFHQ dataset. During this phase, the added channels of the GAN layers are not yet used by the encoder and the GAN generator network is encouraged to learn ignoring signals from these noise channels by just providing random noise for these inputs. Thus, in this phase the noise channels play a placeholder role for a subsequent fine-tuning of the GAN prior network. In the second phase of training, the encoder is included, now replacing the random inputs to the GAN by the activations of matching encoder layers.

For the second phase, training the whole architecture, a data set of pairs of low quality (LQ) and high quality (HQ) images was synthesised. HQ images are downgraded to obtain LQ images using blurring, gaussian noise, downsampling and JPEG compression. A weighting of three losses was used to train the GPEN architecture:  $L_1$ , adversarial and LPIPS losses (see Chapter 2.1.1 and 3.2) based on features from discriminator, rather than VGG network.

### 8.2 GFP-GAN: Towards Real-World Blind Face Restoration with Generative Facial Prior

Generative Facial Prior GAN (GFP-GAN) [8] is a framework for real-world blind face restoration applications (see Figure

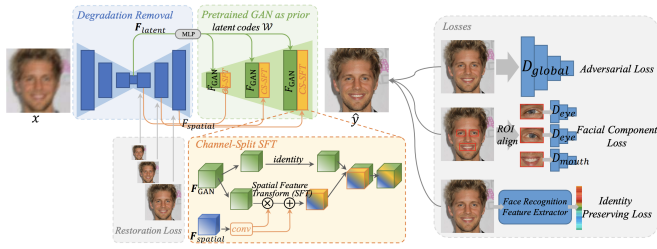


Figure 24: GFP-GAN architecture [8]



Figure 25: Personalized super-resolution results using MyStyle [70] [9]

24). It resembles GPEN (see Chapter 8.1), but employs an a degradation removal module in the form of a U-Net as an encoder, along with with a number of connectivity changes that allow the usage of a pre-trained StyleGAN as a decoder without the need for a training from scratch and subsequent fine-tuning of a modified StyleGAN, as in GPEN.

To achieve this, the U-Net decoder features are fed to a channel split-spatial feature transform (CS-SFT) module that learns to modify activations in StyleGAN layers for better perceptual quality of the generated image with identity preservation. The interaction between the standard StyleGAN and the newly introduce spatial channels are shown in the CS-SFT box within Figure 24. The SFT operation happens as follows. Spatial features from the U-Net go into a convolutional module generating an output tuple  $(\alpha, \beta)$  with parameters for spatial-wise feature modulation. Parameter  $\alpha$  is being used for element-wise scaling of GAN features,  $\beta$  specifies an additive shift. After this, the obtained modulated channels are concatenated with the untouched GAN channels to form the final result, as depicted in box “Channel-Split SFT” in Figure 24.

Again a composition of losses is applied to train the entire architecture. First, motivated from the U-Net, a pixel-wise reconstruction loss  $L_1$  between the degraded input image and ground truth version of the image at different scales (see the blue U-Net in Figure 24) is used. Second, the restored output image  $\hat{Y}$  of the StyleGAN generator can be compared with the degraded input image  $X$  using LPIPS, and Identity losses (see Chapter 3). Third, since the eyes and mouth are crucial to a person’s personality, a further Facial Component loss is introduced which consists of local discriminators for the left eye, right eye, mouth, and the complete face. The Region of Interest Align operator provides these discriminators with corresponding regions of the generated face.

### 8.3 MyStyle: A Personalized Generative Prior

We have described this architecture [70] [9] already in some detail in Chapter 5.4.2. Here, from the perspective of HQ face image restoration, we only remark that this architecture also applies a StyleGAN to solve the problem of super-resolution, using  $L_2$  pixel and LPIPS losses, with a down-

## Deep Fake types

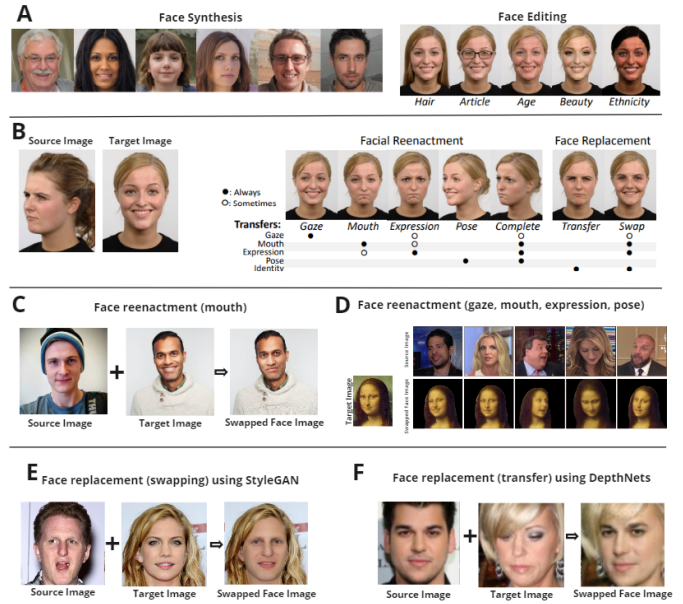


Figure 26: A) Face Synthesis and editing examples [28], B) Description of the types of deepfakes [28], C) Face Reenactment of the mouth [31], D) complete face reenactment [32], E) Face swapping utilizing StyleGAN [14], F) Face Transfer using DepthNets [33].

scaling operation applied to the images before application of these losses.

## 9 DEEPFAKES

*Deepfake* is the manipulation of an image of a face that is hardly recognizable by humans. Deepfake creation methods can be classified into the following types (Fig. 26):

**Synthesis:** a deepfake face is created without a face image. Chapter 2 covers the synthesis of photo-realistic fake images of faces that do not exist.

**Editing:** facial features of are altered, added or removed (see Chapter 6).

**Reenactment:** a source face is used to control gaze, mouth or expression of a target face [77] [78] [32]. Following articles focus on mouth reenactment [79] [80], gaze reenactment [81], and pose reenactment [82].

**Replacement:** the identity of the source face is used to replace the identity of the target face [83] [84] [85].

**Replacement (Transfer):** the identity and expression of the source face is used to replace the identity and expression of the target face, which can be perceived as consecutive face swapping and face reenactment [33].

This chapter will focus on **reenactment** (Chapters 9.1) and **replacement** (Chapter 9.2) methods. The main difference between face reenactment and face replacement is that in face replacement, the identity of the source face is transferred to the target face.

### 9.1 Facial Reenactment

Face reenactment (see Figure 26B) is useful in the advertisement or in the film industry [28]. Typically, if the main actor

(target) has limited time or high costs, another substitute actor (source) can perform the acting and the expressions are then transferred to the main actors face, as if he or she is actually performing [86]. In this case, the main actor’s face would be the target face and the substitute actor would be the source. One usage of mouth reenactment could be voice dubbing into another language for advertisements, music or video games. Gaze reenactment can be used to improve photographs by making the people (target) look into the camera (or where desired) [87]. Pose reenactment has been used for face frontalization in security footage (target) to improve face recognition [88].

Facial reenactment can be realized by the StyleGAN and its latent code. For instance, for transferring expression from a source image  $x_s$  to a target image  $x_t$  the authors of [31] solve the following optimization problem to find the latent code  $s_r$  of the desired result image:

$$s_r = \underset{s}{\operatorname{argmin}} [D_1(G(s), x_s) + D_2(G(s), x_t)].$$

Here,  $G(\cdot)$  is the mapping function of the generator, and  $D_1(x, x')$ ,  $D_2(x, x')$  are suitable distance functions in image space that measure similarity of a face image pair w.r.t. expression ( $D_1$ ) and appearance ( $D_2$ ) of the faces.

To solve this equation the authors constrain the solution space to particular linear combinations  $s_r = \alpha s_s + \beta s_t$  of the StyleGAN latent codes of the given images. Here,  $\alpha$  and  $\beta = 1 - \alpha$  are diagonal  $18 \times 18$  matrices whose diagonal elements may only attain values 0 or 1. This is equivalent to adopting for the 18 style parameters of  $s_r$  either the corresponding value of  $s_s$  or  $s_t$ , leading to a finite search space of  $2^{18}$  possibilities for the optimization problem. From their solutions, they discover that StyleGAN layer 4 is primarily responsible for expression, while other layers (e.g. 8 and 9) control primarily hair color and hat style [31].

## 9.2 Face Replacement and Face Transfer

Face replacement and face transfer are closely related. While face replacement swaps a face into the position of a previous face, face transfer additionally takes care to make the swapped face inherit the expression of the previous face, which is usually achieved with an additional face reenactment step.

Face replacement can be established using classical computer graphics-based approaches [89] by using facial landmarks extracted for each face. The results however are not as good as using neural network based methods.

FakeApp [83] used an encoder-decoder NN architecture to swap faces of two different people A and B. Expressions and emotions from the target image are kept, while the facial identity is swapped. First, it collects a dataset of faces of two people, A and B, using an object detection method [90]. Secondly, it trains two auto-encoders  $E_A$ ,  $E_B$  to encode and two decoder  $D_A$ ,  $D_B$  to reconstruct the faces of A and B respectively. The key idea is that the two encoders have to share the same weights, but they keep their respective decoder weights independent. This allows the encoder to learn global features of the two faces A and B while the two decoders are trained to use this general encoding to generate face specific details of person A or B respectively. Thirdly, to create the face swap, trained encoder  $E_A$  and decoder

$D_B$  are used for the images of person A. This method is applicable for videos as well. The results are similar to Figure 26e) and f). The downside of this approach is, the large dataset of faces of both people that is needed to train the encoder-decoder networks. When using this method on videos, a big problem is the temporal coherence. As this method does not take preceding frames into account, it may produce flickering of the faces. This can be mitigated by providing context, implementing temporal coherence losses [91] [92].

The Face Transfer Module (FTM) [14] mitigates most of the problems described above. It can transfer faces without ever having seen them before. The expression of the face of the target image remains, but the facial identity is transferred from the target image (see Figure 26D). It uses a trained StyleGAN model as a decoder and employs the Hierarchical Representation Face Encoder (HieRFE), [14] which is based on the ResNet50 network, to project images of faces into the improved latent space of StyleGAN with transformers [93].

Another approach [33] tries to predict the 3D pose of the face and its facial landmarks from the 2D source image and predicting the rotation and translation of the landmarks to map them onto the facial landmarks of the target image. For predicting the 3D poses of the facial landmarks, [33] uses an unsupervised Siamese-like network [94] consisting of convolutions, pooling layers, and densely connected layers that they named *DepthNet*. The two images pass through the network which then predicts the depth and affine transformation to map one face onto the other. A CycleGAN [95] is used to cleanly blend the new face position into the image.

## 10 CONCLUSION

With their properties, GANs are the most interesting model for working in the faces domain. As a result of the breakthroughs and refinements described above, GANs have become the preferred type of models for the generation of high quality face images. For this task, they have been extensively studied and optimized, and are comparably well understood.

A notable drawback is that the training can become computationally very expensive (not seldom an order of magnitude higher than most other approaches). However, many applications do not require a training from scratch and can work with StyleGANs only as embedded and fixed, pretrained modules, causing only much lighter computational burden.

Moreover, GANs in the form of StyleGANs are among the best-optimized architectures not only for face generation but with regard to offering rich and flexible control of the generation process. This is due to their rich and well-optimized latent spaces that lend themselves to fine hierarchical control of the face image control process, allowing to correlate changes in the latent space with semantic properties in the image. Moreover, many of these favorable properties have also been found to hold for domains other than faces. This has opened up a wealth of different applications in which GANs, and particular StyleGANs play a central role.



## REFERENCES

- [1] "This person does not exist," <https://thispersondoesnotexist.com>.
- [2] "Gan folks," <https://opensea.io/collection/ganfolk>.
- [3] T. Karras, S. Laine, M. Aittala, J. Hellsten, J. Lehtinen, and T. Aila, "Analyzing and improving the image quality of stylegan," in *Proceedings of the IEEE/CVF conference on computer vision and pattern recognition*, 2020, pp. 8110–8119.
- [4] T. Karras, M. Aittala, J. Hellsten, S. Laine, J. Lehtinen, and T. Aila, "Training generative adversarial networks with limited data," *Advances in Neural Information Processing Systems*, vol. 33, pp. 12 104–12 114, 2020.
- [5] T. Karras, S. Laine, and T. Aila, "A style-based generator architecture for generative adversarial networks," in *Proceedings of the IEEE/CVF conference on computer vision and pattern recognition*, 2019, pp. 4401–4410.
- [6] O. Patashnik, Z. Wu, E. Shechtman, D. Cohen-Or, and D. Lischinski, "Styleclip: Text-driven manipulation of stylegan imagery," in *Proceedings of the IEEE/CVF International Conference on Computer Vision*, 2021, pp. 2085–2094.
- [7] R. Abdal, Y. Qin, and P. Wonka, "Image2stylegan++: How to edit the embedded images?" in *Proceedings of the IEEE/CVF conference on computer vision and pattern recognition*, 2020, pp. 8296–8305.
- [8] X. Wang, Y. Li, H. Zhang, and Y. Shan, "Towards real-world blind face restoration with generative facial prior," in *Proceedings of the IEEE/CVF Conference on Computer Vision and Pattern Recognition*, 2021, pp. 9168–9178.
- [9] Y. Nitzan, K. Aberman, Q. He, O. Liba, M. Yarom, Y. Gandelman, I. Mosseri, Y. Pritch, and D. Cohen-Or, "Mystyle: A personalized generative prior," *arXiv preprint arXiv:2203.17272*, 2022.
- [10] "My style examples," <https://mystyle-personalized-prior.github.io/>.
- [11] "Toonify.photos," <https://toonify.photos/>.
- [12] R. Gal, O. Patashnik, H. Maron, G. Chechik, and D. Cohen-Or, "Stylegan-nada: Clip-guided domain adaptation of image generators," *CoRR*, vol. abs/2108.00946, 2021. [Online]. Available: <https://arxiv.org/abs/2108.00946>
- [13] A. Tewari, M. Elgharib, G. Bharaj, F. Bernard, H.-P. Seidel, P. Pérez, M. Zollhofer, and C. Theobalt, "Stylerig: Rigging stylegan for 3d control over portrait images," in *Proceedings of the IEEE/CVF Conference on Computer Vision and Pattern Recognition*, 2020, pp. 6142–6151.
- [14] Y. Zhu, Q. Li, J. Wang, C. Xu, and Z. Sun, "One shot face swapping on megapixels," *2021 IEEE/CVF Conference on Computer Vision and Pattern Recognition (CVPR)*, pp. 4832–4842, 2021.
- [15] H. Luo, K. Nagano, H. W. Kung, Q. Xu, Z. Wang, L. Wei, L. Hu, and H. Li, "Normalized avatar synthesis using stylegan and perceptual refinement," in *Proceedings of the IEEE/CVF Conference on Computer Vision and Pattern Recognition*, 2021, pp. 11 662–11 672.
- [16] J. Parvizi, C. Jacques, B. L. Foster, N. Withoft, V. Rangarajan, K. S. Weiner, and K. Grill-Spector, "Electrical stimulation of human fusiform face-selective regions distorts face perception," *Journal of Neuroscience*, vol. 32, no. 43, pp. 14 915–14 920, 2012.
- [17] A. Melnik, P. Legkov, K. Izdebski, S. M. Kärcher, W. D. Hairston, D. P. Ferris, and P. König, "Systems, subjects, sessions: to what extent do these factors influence eeg data?" *Frontiers in human neuroscience*, vol. 11, p. 150, 2017.
- [18] "Facial features report," [https://www.cryobank.com/\\_resources/pdf/sampleinformation/facialfeaturesample.pdf](https://www.cryobank.com/_resources/pdf/sampleinformation/facialfeaturesample.pdf), accessed: 2022-10-10.
- [19] A. Melnik, E. Akbulut, J. Sheikh, K. Loos, M. Buettner, and T. Lenze, "Faces: Ai blitz xiii solutions," *arXiv preprint arXiv:2204.01081*, 2022.
- [20] "Gan folks medium," <https://towardsdatascience.com/ganfolk-using-ai-to-create-portraits-of-fictional-people-to-sell-as-nft-46275514e811>.
- [21] Y. Alaluf, O. Patashnik, Z. Wu, A. Zamir, E. Shechtman, D. Lischinski, and D. Cohen-Or, "Third time's the charm? image and video editing with stylegan3," *arXiv preprint arXiv:2201.13433*, 2022.
- [22] T. Karras, M. Aittala, S. Laine, E. Härkönen, J. Hellsten, J. Lehtinen, and T. Aila, "Alias-free generative adversarial networks," *Advances in Neural Information Processing Systems*, vol. 34, 2021.
- [23] A. Radford, J. W. Kim, C. Hallacy, A. Ramesh, G. Goh, S. Agarwal, G. Sastry, A. Askell, P. Mishkin, J. Clark et al., "Learning transferable visual models from natural language supervision," in *International Conference on Machine Learning*. PMLR, 2021, pp. 8748–8763.
- [24] W. Jang, G. Ju, Y. Jung, J. Yang, X. Tong, and S. Lee, "Stylecarigan: caricature generation via stylegan feature map modulation," *ACM Transactions on Graphics (TOG)*, vol. 40, no. 4, pp. 1–16, 2021.
- [25] H. Wang, G. Lin, S. C. Hoi, and C. Miao, "3d cartoon face generation with controllable expressions from a single gan image," *arXiv preprint arXiv:2207.14425*, 2022.
- [26] J. Back, "Fine-tuning stylegan2 for cartoon face generation," *arXiv preprint arXiv:2106.12445*, 2021.
- [27] T. T. Nguyen, Q. V. H. Nguyen, D. T. Nguyen, D. T. Nguyen, T. Huynh-The, S. Nahavandi, T. T. Nguyen, Q.-V. Pham, and C. M. Nguyen, "Deep learning for deepfakes creation and detection: A survey," *Computer Vision and Image Understanding*, vol. 223, p. 103525, 2022.
- [28] Y. Mirsky and W. Lee, "The creation and detection of deepfakes: A survey," *ACM Computing Surveys (CSUR)*, vol. 54, no. 1, pp. 1–41, 2021.
- [29] "Deep nostalgia," <https://www.myheritage.com/deep-nostalgia>, accessed: 2022-09-18.
- [30] L. Verdoliva, "Media forensics and deepfakes: An overview," *IEEE Journal of Selected Topics in Signal Processing*, vol. 14, pp. 910–932, 2020.
- [31] C. Yang and S.-N. Lim, "Unconstrained facial expression transfer using style-based generator," *ArXiv*, vol. abs/1912.06253, 2019.
- [32] E. Burkov, I. Pasechnik, A. Grigorev, and V. Lempitsky, "Neural head reenactment with latent pose descriptors," in *2020 IEEE/CVF Conference on Computer Vision and Pattern Recognition (CVPR)*, 2020, pp. 13 783–13 792.
- [33] J. R. A. Moniz, C. Beckham, S. Rajotte, S. Honari, and C. Pal, "Unsupervised depth estimation, 3d face rotation and replacement," *Advances in neural information processing systems*, vol. 31, 2018.
- [34] A. G. Howard, M. Zhu, B. Chen, D. Kalenichenko, W. Wang, T. Weyand, M. Andreetto, and H. Adam, "Mobilenets: Efficient convolutional neural networks for mobile vision applications," *ArXiv*, vol. abs/1704.04861, 2017.
- [35] M. Li, J. Lin, Y. Ding, Z. Liu, J.-Y. Zhu, and S. Han, "Gan compression: Efficient architectures for interactive conditional gans," in *Proceedings of the IEEE/CVF Conference on Computer Vision and Pattern Recognition*, 2020.
- [36] Y. Viazovetskyi, V. Ivashkin, and E. Kashin, "Stylegan2 distillation for feed-forward image manipulation," in *European conference on computer vision*. Springer, 2020, pp. 170–186.
- [37] I. Goodfellow, J. Pouget-Abadie, M. Mirza, B. Xu, D. Warde-Farley, S. Ozair, A. Courville, and Y. Bengio, "Generative adversarial networks," *Communications of the ACM*, vol. 63, no. 11, pp. 139–144, 2020.
- [38] M. Arjovsky, S. Chintala, and L. Bottou, "Wasserstein generative adversarial networks," in *International conference on machine learning*. PMLR, 2017, pp. 214–223.
- [39] J. H. Lim and J. C. Ye, "Geometric gan," *arXiv preprint arXiv:1705.02894*, 2017.
- [40] N. Kodali, J. Abernethy, J. Hays, and Z. Kira, "On convergence and stability of gans," *arXiv preprint arXiv:1705.07215*, 2017.
- [41] T. Karras, T. Aila, S. Laine, and J. Lehtinen, "Progressive growing of gans for improved quality, stability, and variation," in *International Conference on Learning Representations*, 2018.
- [42] X. Huang and S. Belongie, "Arbitrary style transfer in real-time with adaptive instance normalization," in *2017 IEEE International Conference on Computer Vision (ICCV)*, 2017, pp. 1510–1519.
- [43] R. Xu, X. Wang, K. Chen, B. Zhou, and C. C. Loy, "Positional encoding as spatial inductive bias in gans," in *Proceedings of the IEEE/CVF Conference on Computer Vision and Pattern Recognition*, 2021, pp. 13 569–13 578.
- [44] "Flickr-faces-hq dataset github," <https://github.com/NVlabs/ffhq-dataset>.
- [45] Z. Li, P. Luo, X. Wang, and X. Tang, "Deep learning face attributes in the wild," in *Proceedings of the IEEE international conference on computer vision*, 2015, pp. 3730–3738.
- [46] D. E. King, "Dlib-ml: A machine learning toolkit," *Journal of Machine Learning Research*, vol. 10, pp. 1755–1758, 2009.
- [47] Y. Blau and T. Michaeli, "The perception-distortion tradeoff," in *Proceedings of the IEEE conference on computer vision and pattern recognition*, 2018, pp. 6228–6237.
- [48] R. Zhang, P. Isola, A. A. Efros, E. Shechtman, and O. Wang, "The unreasonable effectiveness of deep features as a perceptual metric," in *Proceedings of the IEEE Conference on Computer Vision and Pattern Recognition (CVPR)*, 6 2018.

- [49] K. Simonyan and A. Zisserman, "Very deep convolutional networks for large-scale image recognition," 2015.
- [50] A. Krizhevsky, I. Sutskever, and G. E. Hinton, "Imagenet classification with deep convolutional neural networks," *Communications of the ACM*, vol. 60, no. 6, pp. 84–90, 2017.
- [51] J. Deng, J. Guo, N. Xue, and S. Zafeiriou, "Arcface: Additive angular margin loss for deep face recognition," in *Proceedings of the IEEE/CVF conference on computer vision and pattern recognition*, 2019, pp. 4690–4699.
- [52] M. Heusel, H. Ramsauer, T. Unterthiner, B. Nessler, and S. Hochreiter, "Gans trained by a two time-scale update rule converge to a local nash equilibrium," *Advances in neural information processing systems*, vol. 30, 2017.
- [53] C. Szegedy, V. Vanhoucke, S. Ioffe, J. Shlens, and Z. Wojna, "Rethinking the inception architecture for computer vision," in *Proceedings of the IEEE conference on computer vision and pattern recognition*, 2016, pp. 2818–2826.
- [54] A. H. Bermano, R. Gal, Y. Alaluf, R. Mokady, Y. Nitzan, O. Tov, O. Patashnik, and D. Cohen-Or, "State-of-the-art in the architecture, methods and applications of stylegan," in *Computer Graphics Forum*, vol. 41, no. 2. Wiley Online Library, 2022, pp. 591–611.
- [55] Z. Wu, D. Lischinski, and E. Shechtman, "StyleSpace analysis: Disentangled controls for stylegan image generation," 2021 *IEEE/CVF Conference on Computer Vision and Pattern Recognition (CVPR)*, pp. 12 858–12 867, 2021.
- [56] E. Richardson, Y. Alaluf, O. Patashnik, Y. Nitzan, Y. Azar, S. Shapiro, and D. Cohen-Or, "Encoding in style: a stylegan encoder for image-to-image translation," in *Proceedings of the IEEE/CVF conference on computer vision and pattern recognition*, 2021, pp. 2287–2296.
- [57] O. Tov, Y. Alaluf, Y. Nitzan, O. Patashnik, and D. Cohen-Or, "Designing an encoder for stylegan image manipulation," *ACM Transactions on Graphics (TOG)*, vol. 40, pp. 1 – 14, 2021.
- [58] Y. Alaluf, O. Patashnik, and D. Cohen-Or, "Restyle: A residual-based stylegan encoder via iterative refinement," in *Proceedings of the IEEE/CVF International Conference on Computer Vision*, 2021, pp. 6711–6720.
- [59] D. Roich, R. Mokady, A. H. Bermano, and D. Cohen-Or, "Pivotal tuning for latent-based editing of real images," *ACM Transactions on Graphics (TOG)*, vol. 42, no. 1, pp. 1–13, 2022.
- [60] Y. Alaluf, O. Tov, R. Mokady, R. Gal, and A. Bermano, "Hyperstyle: Stylegan inversion with hypernetworks for real image editing," in *Proceedings of the IEEE/CVF Conference on Computer Vision and Pattern Recognition*, 2022, pp. 18 511–18 521.
- [61] Z. C. Lipton and S. Tripathi, "Precise recovery of latent vectors from generative adversarial networks," *ArXiv*, vol. abs/1702.04782, 2017.
- [62] S. Garfield, "Official portrait of president-elect barack obama," 2009, published under CC BY 2.0.
- [63] V. S. Photography, "Actors headshots female white late twenties," 2016, published under CC BY 2.0.
- [64] J. Johnson, A. Alahi, and L. Fei-Fei, "Perceptual losses for real-time style transfer and super-resolution," in *European conference on computer vision*. Springer, 2016, pp. 694–711.
- [65] S. Guan, Y. Tai, B. Ni, F. Zhu, F. Huang, and X. Yang, "Collaborative learning for faster stylegan embedding," *ArXiv*, vol. abs/2007.01758, 2020.
- [66] Z. Wang, A. Bovik, H. Sheikh, and E. Simoncelli, "Image quality assessment: from error visibility to structural similarity," *IEEE Transactions on Image Processing*, vol. 13, no. 4, pp. 600–612, 2004.
- [67] T. Wei, D. Chen, W. Zhou, J. Liao, W. Zhang, L. Yuan, G. Hua, and N. Yu, "E2style: Improve the efficiency and effectiveness of stylegan inversion," *IEEE Transactions on Image Processing*, vol. 31, pp. 3267–3280, 2022.
- [68] J. Zhu, Y. Shen, D. Zhao, and B. Zhou, "In-domain gan inversion for real image editing," in *Computer Vision—ECCV 2020: 16th European Conference, Glasgow, UK, August 23–28, 2020, Proceedings, Part XVII*, 2020, pp. 592–608.
- [69] J. Donahue, P. Krähenbühl, and T. Darrell, "Adversarial feature learning," *arXiv preprint arXiv:1605.09782*, 2016.
- [70] A. Melnik and M. Miasoedenkov, "[explained] mystyle: A personalized generative prior," 2022, <https://youtu.be/8YVSIDcFjaI>.
- [71] Y. Shen, J. Gu, X. Tang, and B. Zhou, "Interpreting the latent space of gans for semantic face editing," in *CVPR*, 2020.
- [72] E. Härkönen, A. Hertzmann, J. Lehtinen, and S. Paris, "Ganspace: Discovering interpretable gan controls," *Advances in Neural Information Processing Systems*, vol. 33, pp. 9841–9850, 2020.
- [73] J. N. Pinkney and D. Adler, "Resolution dependent gan interpolation for controllable image synthesis between domains," *arXiv preprint arXiv:2010.05334*, 2020.
- [74] M. Liu, Q. Li, Z. Qin, G. Zhang, P. Wan, and W. Zheng, "Blendgan: implicitly gan blending for arbitrary stylized face generation," *Advances in Neural Information Processing Systems*, vol. 34, pp. 29 710–29 722, 2021.
- [75] J. Back, "Fine-tuning stylegan2 for cartoon face generation," *ArXiv*, vol. abs/2106.12445, 2021.
- [76] T. Yang, P. Ren, X. Xie, and L. Zhang, "Gan prior embedded network for blind face restoration in the wild," in *Proceedings of the IEEE/CVF Conference on Computer Vision and Pattern Recognition*, 2021, pp. 672–681.
- [77] J. Thies, M. Zollhofer, M. Stamminger, C. Theobalt, and M. Nießner, "Face2face: Real-time face capture and reenactment of rgb videos," in *Proceedings of the IEEE conference on computer vision and pattern recognition*, 2016, pp. 2387–2395.
- [78] S. Tulyakov, M.-Y. Liu, X. Yang, and J. Kautz, "Mocogan: Decomposing motion and content for video generation," 2018 *IEEE/CVF Conference on Computer Vision and Pattern Recognition*, pp. 1526–1535, 2018.
- [79] Y. Song, J. Zhu, D. Li, A. Wang, and H. Qi, "Talking face generation by conditional recurrent adversarial network," in *Proceedings of the 28th International Joint Conference on Artificial Intelligence*, 2019, pp. 919–925.
- [80] L. Yu, J. Yu, and Q. Ling, "Mining audio, text and visual information for talking face generation," in 2019 *IEEE International Conference on Data Mining (ICDM)*, 2019, pp. 787–795.
- [81] D. Kononenko, Y. Ganin, D. Sungatullina, and V. Lempitsky, "Photorealistic monocular gaze redirection using machine learning," *IEEE Transactions on Pattern Analysis and Machine Intelligence*, vol. 40, no. 11, pp. 2696–2710, 2018.
- [82] L. Tran, X. Yin, and X. Liu, "Representation learning by rotating your faces," *IEEE Transactions on Pattern Analysis and Machine Intelligence*, vol. 41, pp. 3007–3021, 2019.
- [83] "Fakeapp," <https://www.malavida.com/en/soft/fakeapp/>.
- [84] J. Zhang, X. Zeng, Y. Pan, Y. Liu, Y. Ding, and C. Fan, "Faceswap-net: Landmark guided many-to-many face reenactment," *ArXiv*, vol. abs/1905.11805, 2019.
- [85] L. Li, J. Bao, H. Yang, D. Chen, and F. Wen, "Advancing high fidelity identity swapping for forgery detection," in 2020 *IEEE/CVF Conference on Computer Vision and Pattern Recognition (CVPR)*, 2020, pp. 5073–5082.
- [86] "How deepfake technology can change the movie industry," <https://screenrant.com/movies-deepfake-technology-change-hollywood-how/>, accessed: 2022-09-26.
- [87] "Lip-syncing thanks to artificial intelligence," <https://www.mpg.de/12226519/synchronisation-facial-expressions-video>, accessed: 2022-10-17.
- [88] Y. Liu and J. Chen, "Unsupervised face frontalization using disentangled representation-learning cyclegan," *Computer Vision and Image Understanding*, vol. 222, p. 103526, 2022. [Online]. Available: <https://www.sciencedirect.com/science/article/pii/S1077314222001096>
- [89] Y. Zhang, L. Zheng, and V. L. L. Thing, "Automated face swapping and its detection," in 2017 *IEEE 2nd International Conference on Signal and Image Processing (ICSIP)*, 2017, pp. 15–19.
- [90] C. Limberg, A. Melnik, A. Harter, and H. J. Ritter, "Yolo-you only look 10647 times," *arXiv preprint arXiv:2201.06159*, 2022.
- [91] K. Vougioukas, S. Petridis, and M. Pantic, "End-to-end speech-driven facial animation with temporal gans," in *BMVC*, 2018.
- [92] T.-C. Wang, M.-Y. Liu, J.-Y. Zhu, G. Liu, A. Tao, J. Kautz, and B. Catanzaro, "Video-to-video synthesis," in *NeurIPS*, 2018.
- [93] H. Li, J. Liu, Y. Bai, H. Wang, and K. Mueller, "Transforming the latent space of stylegan for real face editing," *ArXiv*, vol. abs/2105.14230, 2022.
- [94] J. Bromley, I. Guyon, Y. LeCun, E. Säckinger, and R. Shah, "Signature verification using a "siamese" time delay neural network," in *Proceedings of the 6th International Conference on Neural Information Processing Systems*, ser. NIPS'93. San Francisco, CA, USA: Morgan Kaufmann Publishers Inc., 1993, p. 737–744.
- [95] J. Zhu, T. Park, P. Isola, and A. A. Efros, "Unpaired image-to-image translation using cycle-consistent adversarial networks," *CoRR*, vol. abs/1703.10593, 2017. [Online]. Available: <http://arxiv.org/abs/1703.10593>